

SECOND-ORDER RAYLEIGH–SCHRÖDINGER PERTURBATION THEORY FOR THE GRASP2018 PACKAGE: CORE–CORE CORRELATIONS*

G. Gaigalas, P. Rynkun, and L. Kitovienė

Institute of Theoretical Physics and Astronomy, Vilnius University, Saulėtekio 3, 10257 Vilnius, Lithuania

Email: gediminas.gaigalas@tfai.vu.lt; pavel.rynkun@tfai.vu.lt; laima.radziute@tfai.vu.lt

Received 28 May 2024; accepted 15 July 2024

GRASP package is based on the relativistic configuration interaction in which accurate calculations, accounting for valence, valence–valence, core–valence, core and core–core electron correlations, often rely on massive CSF expansions. This paper presents a further development of the method based on the second-order perturbation theory for finding the most important CSFs that have the greatest influence on the core–valence, core and core–core correlations. This method is based on a combination of the relativistic configuration interaction method and the stationary second-order Rayleigh–Schrödinger many-body perturbation theory in an irreducible tensorial form [G. Gaigalas, P. Rynkun, and L. Kitovienė, Second-order Rayleigh–Schrödinger perturbation theory for the GRASP2018 package: Core–valence correlations, *Lith. J. Phys.* **64**(1), 20–39 (2024), <https://doi.org/10.3952/physics.2024.64.1.3>, and G. Gaigalas, P. Rynkun, and L. Kitovienė, Second-order Rayleigh–Schrödinger perturbation theory for the GRASP2018 package: Core correlations, *Lith. J. Phys.* **64**(2), 73–81 (2024), <https://doi.org/10.3952/physics.2024.64.2.1>]. In this extension, the perturbation theory takes into account electron core–valence, core and core–core correlations, where an atom or ion has any number of valence electrons, for calculation of energy spectra and other properties. Meanwhile, the rest of the correlations are taken into account in a traditional way. This allows a significant reduction of the space of the configuration state function for complex atoms and ions. We also demonstrate how this method works for calculations of the energy structure and E1 transition properties of Fe XV ion.

Keywords: configuration interaction, spin-angular integration, perturbation theory, tensorial algebra, core–core correlations, core–valence correlations, core correlations

1. Introduction

This paper describes the method, an extension to the approach presented in Refs. [1, 2], that allows atomic structure calculations to be performed faster and with the use of less resources in the framework of relativistic atomic theory. The method is based on a combination of the relativistic configuration interaction (RCI) method [3, 4] and on the stationary second-order Rayleigh–Schrödinger many-body perturbation theory (for the non-relativistic version of this perturbation theory in

determinants, see Ref. [5]) in an irreducible tensorial form (for the non-relativistic version of this perturbation theory in an irreducible tensorial form, see Refs. [6–8]). In this extension, the perturbation theory takes into account electron core–valence (CV), core (C) and core–core (CC) correlations where an atom or ion has any number of valence electrons, meanwhile the rest of the correlations are taken into account in a traditional way.

GRASP [9, 10] is based on the relativistic configuration interaction, and the wave functions of the targeted states are given as expansions over configuration state functions (CSF) built on relativistic one-electron orbitals [11]. Accurate RCI calculations, considering valence, valence–valence, core–valence, core and core–core electron

* Dedicated to the memory of professor **Adolfas Jucys** (1904–1974), pioneer of contemporary theoretical physics in Lithuania, initiator of the ‘Lithuanian Physics Collection’, on the occasion of his birth and death anniversaries.

correlations, often rely on massive CSF expansions obtained from single- and double (SD) excitations from a multireference (MR) consisting of the most important configurations [4]. Our proposed approach uses the second-order perturbation theory to find the most important CSFs that have the greatest influence on the core–valence, core and core–core correlations. This reduces the CSF base, on the one hand, while, on the other hand, it allows the calculation of the energy structure, transition characteristics and other properties of atoms and ions to be carried out without loss of accuracy. Since GRASP uses the formalism of tensorial algebra [12], only Rayleigh–Schrödinger many-body perturbation theory (RSMBPT) in an irreducible tensorial form can be used in it. This makes the work unique and makes it necessary to have the expressions for the Feynman diagrams in an irreducible tensorial form. It is possible to obtain them by using the combination of the angular momentum theory, the concept of irreducible tensorial sets, the generalized graphical approach and the second quantization in a coupling tensorial form [13, 14]. All these expressions for the Feynman diagrams corresponding to core–core correlations in the relativistic atomic theory are first presented in Section 2. In order to be able to use the spin-angular program library [12] without any further modification, these formulas have

first been adapted in a way that is aligned with GRASP [9, 10]. They are given in Section 3. Meanwhile, a similar study on core–valence and core correlations was first done in our previous work [1, 2]. Both studies make a full use of Racah algebra including a quasispin [14] for the integration of spin-angular part of all these types (core–valence, core and core–core) of correlations. The validity and efficiency of the presented method is demonstrated in Section 4, where the energy spectrum and E1 transition properties of the Fe XV ion are theoretically studied.

2. Relativistic second-order effective Hamiltonian of an atom or an ion in an irreducible tensorial form for core–core correlations

All possible core–core correlations can be treated perturbatively including all of them via the RSMBPT method. All types of CC correlations are described below in separate subsections in more detail.

2.1. The first type of core–core correlations

Here we will discuss the first type of core–core correlations which are expressed through vacuum Feynman diagrams CC₁ from Fig. 1 and CC₂ from Fig. 2:

$$CC_1 = \frac{1}{2} \sum_{r,s,a,b} \frac{(-1)^{j_a+j_b+j_r+j_s}}{(\epsilon_a + \epsilon_b - \epsilon_r - \epsilon_s)} \sum_{k,k'} \frac{\delta(k, k')}{\sqrt{[k, k']}} X_k(ab, rs) X_{k'}(rs, ab)$$

Fig. 1. The CC Feynman diagram of the second-order effective Hamiltonian for the direct part of excitation $(n_a \ell_a) j_a^{2j_a+1} (n_b \ell_b) j_b^{2j_b+1} (n_m \ell_m) j_m^{w_m} (n_n \ell_n) j_n^{w_n} \rightarrow (n_a \ell_a) j_a^{2j_a} (n_b \ell_b) j_b^{2j_b} (n_m \ell_m) j_m^{w_m} (n_n \ell_n) j_n^{w_n} (n_s \ell_s) j_s (n_r \ell_r) j_r$, where $a \neq b$ or $a = b$ and $s \neq r$ or $s = r$.

$$CC_2 = \frac{1}{2} \sum_{r,s,a,b} \frac{(-1)^{j_a+j_b+j_r+j_s}}{(\epsilon_a + \epsilon_b - \epsilon_r - \epsilon_s)} \sum_{k,k'} \left\{ \begin{matrix} k & j_a & j_r \\ k' & j_b & j_s \end{matrix} \right\} X_k(ab, rs) X_{k'}(sr, ab)$$

Fig. 2. The CC Feynman diagram of the second-order effective Hamiltonian for the exchange part of excitation $(n_a \ell_a) j_a^{2j_a+1} (n_b \ell_b) j_b^{2j_b+1} (n_m \ell_m) j_m^{w_m} (n_n \ell_n) j_n^{w_n} \rightarrow (n_a \ell_a) j_a^{2j_a} (n_b \ell_b) j_b^{2j_b} (n_m \ell_m) j_m^{w_m} (n_n \ell_n) j_n^{w_n} (n_s \ell_s) j_s (n_r \ell_r) j_r$, where $a \neq b$ or $a = b$ and $s \neq r$ or $s = r$.

$$(n_a \ell_a) j_a^{2j_a+1} (n_b \ell_b) j_b^{2j_b+1} (n_m \ell_m) j_m^{w_m} (n_n \ell_n) j_n^{w_n} \\ \rightarrow (n_a \ell_a) j_a^{j_a} (n_b \ell_b) j_b^{j_b} (n_m \ell_m) j_m^{w_m} (n_n \ell_n) j_n^{w_n} (n_r \ell_r) j_r (n_s \ell_s) j_s \quad (1)$$

$$(n_a \ell_a) j_a^{2j_a+1} (n_b \ell_b) j_b^{2j_b+1} (n_m \ell_m) j_m^{w_m} (n_n \ell_n) j_n^{w_n} \\ \rightarrow (n_a \ell_a) j_a^{j_a} (n_b \ell_b) j_b^{j_b} (n_m \ell_m) j_m^{w_m} (n_n \ell_n) j_n^{w_n} (n_r \ell_r) j_r^2 \quad (2)$$

$$(n_a \ell_a) j_a^{2j_a+1} (n_m \ell_m) j_m^{w_m} (n_n \ell_n) j_n^{w_n} \\ \rightarrow (n_a \ell_a) j_a^{j_a-1} (n_m \ell_m) j_m^{w_m} (n_n \ell_n) j_n^{w_n} (n_r \ell_r) j_r (n_s \ell_s) j_s \quad (3)$$

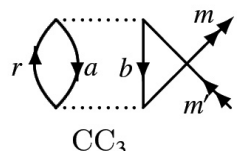
$$(n_a \ell_a) j_a^{2j_a+1} (n_m \ell_m) j_m^{w_m} (n_n \ell_n) j_n^{w_n} \\ \rightarrow (n_a \ell_a) j_a^{j_a-1} (n_m \ell_m) j_m^{w_m} (n_n \ell_n) j_n^{w_n} (n_r \ell_r) j_r^2 \quad (4)$$

These two Feynman diagrams CC_1 and CC_2 are vacuum diagrams without any spin-angular part, therefore the spin-angular program library [12] from GRASP is not needed. They have the same impact on those CSFs that have the same configuration. The diagram CC_1 describes the direct part of excitations (1–4) and CC_2 describes the exchange part of the same excitations.

Each second-order Feynman diagram's expression of Rayleigh–Schrödinger many-body perturbation theory as described in Ref. [1] has the energy denominator $D = \Sigma (\varepsilon_{\text{down}} - \varepsilon_{\text{up}})$, where $\varepsilon_{\text{down}}$ (ε_{up}) is the single-particle eigenvalue associated with the down-(up-) orbital lines to (from) the lowest interaction line of the diagram. For example, the denominators for CC_1 and CC_2 diagrams are

$$D = (\varepsilon_a + \varepsilon_b - \varepsilon_r - \varepsilon_s), \quad (5)$$

where indexes a and b belong to the F set, and r, s belong to the G set of orbitals [1].



$$CC_3 = \sum_{m,m'} \frac{1}{\sqrt{[jm]}} \left[\tilde{a}^{(jm')} \times a^{(jm)} \right]^{(0)} \sum_{r,a,b} \frac{(-1)^{j_a+j_b+j_r+j_m}}{(\varepsilon_a + \varepsilon_b - \varepsilon_r - \varepsilon_m)} \\ \times \sum_{k,k'} \frac{\delta(k,k')}{\sqrt{[k,k']}} X_k(ab, rm') X_{k'}(rm, ab)$$

Fig. 3. The CC Feynman diagram of the second-order effective Hamiltonian for the direct part of excitation $(n_a \ell_a) j_a^{2j_a+1} (n_b \ell_b) j_b^{2j_b+1} (n_m \ell_m) j_m^{w_m} (n_n \ell_n) j_n^{w_n} \rightarrow (n_a \ell_a) j_a^{j_a} (n_b \ell_b) j_b^{j_b} (n_m \ell_m) j_m^{w_m+1} (n_n \ell_n) j_n^{w_n} (n_r \ell_r) j_r$, where $a \neq b$ or $a = b$.

Also, the following notations are used in the expressions of these diagrams (see Figs. 1 and 2):

$$X_k(ij, i'j') = \langle \ell_i j_i || C^{(k)} || \ell_{i'} j_{i'} \rangle \\ \langle \ell_j j_j || C^{(k)} || \ell_{j'} j_{j'} \rangle R^k(n_i j_i n_j j_j n_{i'} j_{i'} n_{j'} j_{j'}), \quad (6)$$

where $R^k(n_i j_i n_j j_j n_{i'} j_{i'} n_{j'} j_{j'})$ is the radial integral of electrostatic interaction between electrons [4, (89) and (90)] and $\langle \ell_i j_i || C^{(k)} || \ell_{i'} j_{i'} \rangle$ is the reduced matrix element of the irreducible tensor operator $C^{(k)}$ in the jj -coupling.

The exchange diagram CC_2 additionally has a $6j$ -coefficient. The summation in the expressions of CC_1 and CC_2 are running over the closed lines of Feynman diagrams and over the ranks k and k' of the irreducible tensor operators $C^{(k)}$ and $C^{(k')}$, respectively.

2.2. The second type of core–core correlations

This type of core–core correlations is expressed through the Feynman diagrams CC_3 from Fig. 3 and CC_4 from Fig. 4, where all lines with a double arrow of diagrams are renamed m , i.e. $m' \equiv m$:

$$(n_a \ell_a) j_a^{2j_a+1} (n_b \ell_b) j_b^{2j_b+1} (n_m \ell_m) j_m^{w_m} (n_n \ell_n) j_n^{w_n} \\ \rightarrow (n_a \ell_a) j_a^{j_a} (n_b \ell_b) j_b^{j_b} (n_m \ell_m) j_m^{w_m+1} (n_n \ell_n) j_n^{w_n} (n_r \ell_r) j_r \quad (7)$$

$$(n_a \ell_a) j_a^{2j_a+1} (n_m \ell_m) j_m^{w_m} (n_n \ell_n) j_n^{w_n} \\ \rightarrow (n_a \ell_a) j_a^{j_a-1} (n_m \ell_m) j_m^{w_m+1} (n_n \ell_n) j_n^{w_n} (n_r \ell_r) j_r \quad (8)$$

These diagrams CC_3 and CC_4 are single particle Feynman diagrams where their tensorial part is expressed through the tensorial product of annihilation $\tilde{a}^{(j)}$ and creation $a^{(j)}$ operators

$$\begin{aligned}
 &= \sum_{m,m'} \frac{1}{\sqrt{[j_m]}} \left[\tilde{a}^{(j_{m'})} \times a^{(j_m)} \right]^{(0)} \sum_{r,a,b} \frac{(-1)^{j_a+j_b+j_r+j_m}}{(\varepsilon_a + \varepsilon_b - \varepsilon_r - \varepsilon_m)} \\
 &\times \sum_{k,k'} \left\{ \begin{matrix} k & j_a & j_m \\ k' & j_b & j_r \end{matrix} \right\} X_k(ba, rm') X_{k'}(rm, ab)
 \end{aligned}$$

Fig. 4. The CC Feynman diagram of the second-order effective Hamiltonian for the exchange part of excitation $(n_a \ell_a) j_a^{2j_a+1} (n_b \ell_b) j_b^{2j_b+1} (n_m \ell_m) j_m^{w_m} (n_n \ell_n) j_n^{w_n} \rightarrow (n_a \ell_a) j_a^{2j_a} (n_b \ell_b) j_b^{2j_b} (n_m \ell_m) j_m^{w_{m+1}} (n_n \ell_n) j_n^{w_n} (n_r \ell_r) j_r$, where $a \neq b$ or $a = b$.

$$[\tilde{a}^{(j_{m'})} \times a^{(j_m)}]^{(0)}. \tag{9}$$

2.3. The third type of core–core correlations

These two operators of the second quantization act on the same subshell m and represent the scalar operator. Therefore, this operator can be expressed through the operator of subshell occupation number \hat{N} on which it acts,

$$[\tilde{a}^{(j_m)} \times a^{(j_m)}]^{(0)} = \frac{[j_m] - \hat{N}_m}{\sqrt{[j_m]}}, \tag{10}$$

or through the hole operator \hat{N}_{hol} of this subshell,

$$[\tilde{a}^{(j_m)} \times a^{(j_m)}]^{(0)} = \frac{\hat{N}_{\text{hol } m}}{\sqrt{[j_m]}}. \tag{11}$$

Therefore, as for the first type of core–core correlation (see Subsection 2.1), there is no need to use the spin-angular program library [12] to calculate these diagrams, as the spin-angular coefficients are expressed through a simple multiplier (see diagram A3 in Ref. [15]). This is one of the advantages of the methodology proposed in this paper.

This type of core–core correlations is expressed through the one-particle Feynman diagram CC_5 from Fig. 5 and through the two-particle Feynman diagram CC_6 from Fig. 6, where all lines with a double arrow of diagrams are renamed m , i.e. $m' \equiv m$ for CC_5 and $m' = n = n' \equiv m$ for CC_6 :

$$\begin{aligned}
 &(n_a \ell_a) j_a^{2j_a+1} (n_b \ell_b) j_b^{2j_b+1} (n_m \ell_m) j_m^{w_m} (n_n \ell_n) j_n^{w_n} \\
 &\rightarrow (n_a \ell_a) j_a^{2j_a} (n_b \ell_b) j_b^{2j_b} (n_m \ell_m) j_m^{w_{m+2}} (n_n \ell_n) j_n^{w_n}, \tag{12}
 \end{aligned}$$

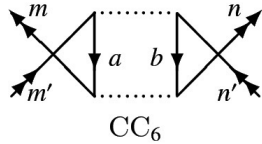
$$\begin{aligned}
 &(n_a \ell_a) j_a^{2j_a+1} (n_m \ell_m) j_m^{w_m} (n_n \ell_n) j_n^{w_n} \\
 &\rightarrow (n_a \ell_a) j_a^{2j_a-1} (n_m \ell_m) j_m^{w_{m+2}} (n_n \ell_n) j_n^{w_n}. \tag{13}
 \end{aligned}$$

The CC_5 diagram has the same tensorial part as the diagrams CC_3 and CC_4 , therefore its spin-angular part can be handled in the same way as for the CC_3 and CC_4 diagrams.

The CC_6 is a two-particle Feynman diagram where its tensorial part is expressed through the tensorial product of annihilation $\tilde{a}^{(j)}$ and creation $a^{(j)}$ operators and represent the scalar operator for this type of core–core correlations

$$\begin{aligned}
 &= \frac{1}{2} \sum_{m,m'} \frac{1}{\sqrt{[j_m]}} \left[\tilde{a}^{(j_{m'})} \times a^{(j_m)} \right]^{(0)} \sum_{n,a,b} \frac{(-1)^{j_a+j_b+j_m+j_n}}{(\varepsilon_a + \varepsilon_b - \varepsilon_m - \varepsilon_n)} \\
 &\times \sum_{k,k'} \left\{ \begin{matrix} k & j_a & j_m \\ k' & j_b & j_n \end{matrix} \right\} X_k(ab, m'n) X_{k'}(mn, ba)
 \end{aligned}$$

Fig. 5. The CC one-particle Feynman diagram of the second-order effective Hamiltonian for the third type $(n_a \ell_a) j_a^{2j_a+1} (n_b \ell_b) j_b^{2j_b+1} (n_m \ell_m) j_m^{w_m} (n_n \ell_n) j_n^{w_n} \rightarrow (n_a \ell_a) j_a^{2j_a} (n_b \ell_b) j_b^{2j_b} (n_m \ell_m) j_m^{w_{m+2}} (n_n \ell_n) j_n^{w_n}$ and the fourth type $(n_a \ell_a) j_a^{2j_a+1} (n_b \ell_b) j_b^{2j_b+1} (n_m \ell_m) j_m^{w_m} (n_n \ell_n) j_n^{w_n} \rightarrow (n_a \ell_a) j_a^{2j_a} (n_b \ell_b) j_b^{2j_b} (n_m \ell_m) j_m^{w_{m+1}} (n_n \ell_n) j_n^{w_n+1}$ of core–core correlations.



$$\begin{aligned}
&= \frac{1}{2} \sum_{m,m'} \sum_{n,n'} \sum_{j_{12}} \sqrt{[j_{12}]} \left[[\tilde{a}^{(j_{m'})} \times a^{(j_m)}]^{(j_{12})} \times [\tilde{a}^{(j_{n'})} \times a^{(j_n)}]^{(j_{12})} \right]^{(0)} \\
&\times \sum_{a,b} \frac{1}{(\varepsilon_a + \varepsilon_b - \varepsilon_m - \varepsilon_n)} \sum_{k,k'} \left\{ \begin{matrix} k & k' & j_{12} \\ m & m' & j_a \end{matrix} \right\} \left\{ \begin{matrix} k & k' & j_{12} \\ n & n' & j_b \end{matrix} \right\} \\
&\times X_k(ab, m' n') X_{k'}(mn, ab)
\end{aligned}$$

Fig. 6. The CC two-particle Feynman diagram of the second-order effective Hamiltonian for the third type $(n_a \ell_a) j_a^{2j_a+1} (n_b \ell_b) j_b^{2j_b+1} (n_m \ell_m) j_m^{w_m} (n_n \ell_n) j_n^{w_n} \rightarrow (n_a \ell_a) j_a^{2j_a} (n_b \ell_b) j_b^{2j_b} (n_m \ell_m) j_m^{w_m+2} (n_n \ell_n) j_n^{w_n}$ and the fourth type $(n_a \ell_a) j_a^{2j_a+1} (n_b \ell_b) j_b^{2j_b+1} (n_m \ell_m) j_m^{w_m} (n_n \ell_n) j_n^{w_n} \rightarrow (n_a \ell_a) j_a^{2j_a} (n_b \ell_b) j_b^{2j_b} (n_m \ell_m) j_m^{w_m+1} (n_n \ell_n) j_n^{w_n+1}$ of core–core correlations.

$$[[\tilde{a}^{(j_m)} \times a^{(j_m)}]^{(j_{12})} \times [\tilde{a}^{(j_n)} \times a^{(j_n)}]^{(j_{12})}]^{(0)}. \quad (14)$$

For this CC_6 diagram, unlike for the other Feynman diagrams considered above, there comes the additional summation, where the summation parameter j_{12} relates the tensor product (14) to the two $6j$ -coefficients. This summation parameter is the intermediate rank of this tensor product.

All operators of the second quantization act on the same subshell m , therefore the tensorial operator (14) can be expressed through simple \hat{N} and \hat{N}_{hol} operators in the case of $j_{12} = 0$:

$$\begin{aligned}
&[[\tilde{a}^{(j_m)} \times a^{(j_m)}]^{(0)} \times [\tilde{a}^{(j_m)} \times a^{(j_m)}]^{(0)}]^{(0)} = \\
&= \frac{([J_m] - \hat{N}_m)^2}{[J_m]} \quad (15)
\end{aligned}$$

or

$$\begin{aligned}
&[[\tilde{a}^{(j_m)} \times a^{(j_m)}]^{(0)} \times [\tilde{a}^{(j_m)} \times a^{(j_m)}]^{(0)}]^{(0)} = \\
&= \frac{\hat{N}_{\text{hol } m}^2}{[J_m]}. \quad (16)
\end{aligned}$$

In that case, for the calculation of CC_6 diagram, we also do not need to use the spin-angular program library [12]. Meanwhile, the program library [12] from GRASP supports the calculation of spin-angular part (14) of the CC_6 Feynman diagram in the case of $j_{12} > 0$ after some simple modifications similar to that of Ref. [13] performed in Section 3. After this modification, the full Racah algebra including a quasispin [14] is available for the integration of spin-angular part of this Feynman diagram. This is another advantage of the methodology proposed in this paper.

2.4. The fourth type of core–core correlations

This type of core–core correlations is presented through the Feynman diagram CC_6 , where all lines with a double arrow of diagrams are renamed in the following way: $m' \equiv m$ and $n' \equiv n$,

$$\begin{aligned}
&(n_a \ell_a) j_a^{2j_a+1} (n_b \ell_b) j_b^{2j_b+1} (n_m \ell_m) j_m^{w_m} (n_n \ell_n) j_n^{w_n} \\
&\rightarrow (n_a \ell_a) j_a^{2j_a} (n_b \ell_b) j_b^{2j_b} (n_m \ell_m) j_m^{w_m+1} (n_n \ell_n) j_n^{w_n+1}, \quad (17)
\end{aligned}$$

$$\begin{aligned}
&(n_a \ell_a) j_a^{2j_a+1} (n_m \ell_m) j_m^{w_m} (n_n \ell_n) j_n^{w_n} \\
&\rightarrow (n_a \ell_a) j_a^{2j_a-1} (n_m \ell_m) j_m^{w_m+1} (n_n \ell_n) j_n^{w_n+1}. \quad (18)
\end{aligned}$$

In this case, the tensorial part of the CC_6 diagram has the form

$$\begin{aligned}
&[[\tilde{a}^{(j_m)} \times a^{(j_m)}]^{(j_{12})} \times \\
&\times [\tilde{a}^{(j_n)} \times a^{(j_n)}]^{(j_{12})}]^{(0)}, \quad (19)
\end{aligned}$$

which can be expressed in the case of $j_{12} = 0$ as

$$\begin{aligned}
&[[\tilde{a}^{(j_m)} \times a^{(j_m)}]^{(0)} \times [\tilde{a}^{(j_n)} \times a^{(j_n)}]^{(0)}]^{(0)} = \\
&= \frac{([J_m] - \hat{N}_m) ([J_n] - \hat{N}_n)}{\sqrt{[J_m, J_n]}}, \quad (20)
\end{aligned}$$

or

$$\begin{aligned}
&[[\tilde{a}^{(j_m)} \times a^{(j_m)}]^{(0)} \times [\tilde{a}^{(j_n)} \times a^{(j_n)}]^{(0)}]^{(0)} = \\
&= \frac{\hat{N}_{\text{hol } m} \hat{N}_{\text{hol } n}}{\sqrt{[J_m, J_n]}}. \quad (21)
\end{aligned}$$

So, for this case we also do not need to use the spin-angular program library [12] for the calculation of the CC_6 diagram. Meanwhile, the program library [12] from GRASP supports the calculation of the spin-angular part (19) of the CC_6 Feynman diagram in the case of $j_{12} > 0$ after some simple modifications similar to that of Ref. [13] performed in Section 3. After this modification, the full Racah algebra including a quasispin [14] is available for the integration of the spin-angular part of this Feynman diagram.

2.5. The contribution of core–core correlations to off-diagonal matrix elements

The main contribution of core–core correlations to off-diagonal matrix elements is in the matrix element $\langle (n_m \ell_m) j_m^m (n_n \ell_n) j_n^{w_n} || \hat{\mathcal{H}}_{\text{Effective}}^{(2)} || (n_m \ell_m) j_m^{w_m-2} (n_n \ell_n) j_n^{w_n+2} \rangle$. The above contribution is derived from the excitation

$$\begin{aligned} & (n_a \ell_a) j_a^{2j_a+1} (n_b \ell_b) j_b^{2j_b+1} (n_m \ell_m) j_m^{w_m} (n_n \ell_n) j_n^{w_n} \\ & \rightarrow (n_a \ell_a) j_a^{2j_a} (n_b \ell_b) j_b^{2j_b} (n_m \ell_m) j_m^{w_m} (n_n \ell_n) j_n^{w_n+2} \end{aligned} \quad (22)$$

and can be described through the same two-particle Feynman diagram (Fig. 6) as above. This type of core–core correlations is presented through the Feynman diagram CC_6 where all lines with a double arrow of diagrams are renamed in the following way: $m \equiv n$, $m' \equiv m$, and $n' \equiv m$. Thus, the tensorial part of the CC_6 diagram has the following form:

$$\begin{aligned} & \left[\left[\tilde{a}^{(j_m)} \times a^{(j_n)} \right]^{(j_{12})} \times \right. \\ & \left. \times \left[\tilde{a}^{(j_m)} \times a^{(j_n)} \right]^{(j_{12})} \right]^{(0)}. \end{aligned} \quad (23)$$

In this case, after some modifications made in Section 3, the Racah algebra [14] and the software library [12] are also fully available.

3. PT implementation in the GRASP2018 [9, 10]

Similar to the CV and C correlations [1, 2], the admixed configurations from CC correlations can be added to the usual energy $E_0(K)$ of the term χJ of the configuration K and can be expressed as the energy $\Delta E_0(KJ)$, which does not depend on the term, and the sum of the product of Slater in-

tegrals and spin-angular coefficients, describing the interaction within open subshells and between them,

$$\begin{aligned} E(K \chi J) &= \\ &= E_0(KJ) + \Delta E_0(KJ) + \\ &+ \sum_{nlj} \sum_{k>0} \tilde{f}_k(\ell j^w, K \chi J) \times \\ &\times \left[\mathcal{F}^k(nlj, nlj) + \Delta \mathcal{F}^k(nlj, nlj) \right] + \\ &+ \sum_{nlj} \sum_{n'l'j'>nlj} \left\{ \sum_{k>0} \tilde{f}_k(\ell j^w \ell' j'^{w'}, K \chi J) \times \right. \\ &\times \left[\mathcal{F}^k(nlj, n'l'j') + \Delta \mathcal{F}^k(nlj, n'l'j') \right] + \\ &+ \sum_k \tilde{g}_k(\ell j^w \ell' j'^{w'}, K \chi J) \left[\mathcal{G}^k(nlj, n'l'j') + \right. \\ &+ \Delta \mathcal{G}^k(nlj, n'l'j') \left. \right] + \\ &+ \sum_k \tilde{v}_k(\ell j^w \ell' j'^{w'}, \ell j^{w-2} \ell' j'^{w'+2}, K \chi JK' \chi' J) \times \\ &\times \left[\mathcal{R}^k(nl j n l j, n'l'j'n'l'j') + \right. \\ &+ \Delta \mathcal{R}^k(nl j n l j, n'l'j'n'l'j') \left. \right\}, \end{aligned} \quad (24)$$

where \tilde{f}_k , \tilde{g}_k and \tilde{v}_k are spin-angular coefficients from which submatrix elements $\langle \ell j || C^{(k)} || \ell' j' \rangle$ are extracted. Therefore, the summation over k runs over all possible values instead of the values which satisfy the triangular condition $(\ell \ell' k)$ as it is in the ordinary case. $\mathcal{F}^k(nlj, n'l'j')$, $\mathcal{G}^k(nlj, n'l'j')$ and $\mathcal{R}^k(nl j n l j, n'l'j'n'l'j')$ are the generalized integrals of the electrostatic interaction between electrons. The definition of $\mathcal{R}^k(nl j n l j, n'l'j'n'l'j')$ is

$$\begin{aligned} & \mathcal{R}^k(ij, i'j') \\ &= \{ [1 + \delta(i, j)] [1 + \delta(i', j')] \}^{-1/2} R^k(n_i j_i n_j j_j, n_i j_i n_j j_j) \\ &\times \langle \ell_i j_i || C^{(k)} || \ell_i j_i \rangle \langle \ell_j j_j || C^{(k)} || \ell_j j_j \rangle, \end{aligned} \quad (25)$$

where $R^k(n_i j_i n_j j_j, n_i j_i n_j j_j)$ is the same radial integral as in Eq. (6). Definitions $\mathcal{F}^k(nlj, n'l'j')$, $\mathcal{G}^k(nlj, n'l'j')$ straightforwardly follow from Eq. (25).

The contribution coming from the CC correlations of the configurations K' to $E(K \chi J)$ in the second order of the perturbation theory can be written from Eq. (24) as

$$\begin{aligned}
\Delta E_{\text{PT(CC)}} &= \Delta \mathcal{E}_0(KJ) + \\
&+ \sum_{nlj} \sum_{k>0} \tilde{f}_k(\ell j^w, K \chi J) \Delta \mathcal{F}^k(nlj, nlj) + \\
&+ \sum_{nlj} \sum_{n'\ell'j'>nlj} \left\{ \sum_{k>0} \tilde{f}_k(\ell j^w \ell' j'^w, K \chi J) \times \right. \\
&\times \Delta \mathcal{F}^k(nlj, n'\ell'j') + \\
&+ \sum_k \tilde{g}_k(\ell j^w \ell' j'^w, K \chi J) \Delta \mathcal{G}^k(nlj, n'\ell'j') + \\
&+ \sum_k \tilde{v}_k(\ell j^w \ell' j'^w, \ell j^{w-2} \ell' j'^{w+2}, K \chi J K' \chi' J) \times \\
&\left. \times \Delta \mathcal{R}^k(nljnlj, n'\ell'j'n'\ell'j') \right\}. \quad (26)
\end{aligned}$$

The contribution of the first two types of CC correlations in the second order of the perturbation theory is expressed only over $\Delta \mathcal{E}_0(KJ)$ (see Table 1). The contributions $\Delta \mathcal{F}^k(nlj, nlj)$, $\Delta \mathcal{F}^k(nlj, n'\ell'j')$, and $\Delta \mathcal{G}^k(nlj, n'\ell'j')$ are equal to zero in these cases. The contributions $\Delta \mathcal{E}_0(KJ)$ can be expressed through \mathcal{A} and \mathcal{C} coefficients (see Table 1) which have the following expressions:

$$\begin{aligned}
\mathcal{A}(x, ij, i'j') &= \\
&= \sum_{k,k'} \begin{Bmatrix} k & k' & x \\ j_i & j_i & j_{i'} \end{Bmatrix} \begin{Bmatrix} k & k' & x \\ j_{j'} & j_{j'} & j_j \end{Bmatrix} \mathcal{P}(kk', ij, i'j'), \quad (27)
\end{aligned}$$

$$\mathcal{C}(x, ij, i'j') = \sum_k \begin{Bmatrix} x & j_i & j_{i'} \\ k & j_j & j_{j'} \end{Bmatrix} \mathcal{Q}(xk, ij, i'j'), \quad (28)$$

where

$$\mathcal{P}(kk', ij, i'j') = \mathcal{R}^k(ij, i'j') \mathcal{R}^{k'}(i'j', ij) \mathcal{O}(K', K), \quad (29)$$

$$\mathcal{Q}(kk', ij, i'j') = \mathcal{R}^k(ij, i'j') \mathcal{R}^{k'}(i'j', ji) \mathcal{O}(K', K), \quad (30)$$

and

$$\mathcal{O}(K', K) = \frac{1}{\bar{E}(K') - \bar{E}(K)}, \quad (31)$$

where $\bar{E}(K)$ is the averaged energy of the state for which calculations are performed. $\bar{E}(K')$ is the averaged energy for the admixed configuration K' . For how to find $\bar{E}(K)$ and $\bar{E}(K')$, see Section 3 in Ref. [1]. We would like to emphasize that the energy denominator (31) is defined differently/opposite

Table 1. Expressions for the first (where $a \neq b$ or $a = b$ and $s \neq r$ or $s = r$) and second (where $a \neq b$ or $a = b$) types of core–core corrections to the energy in Eq. (24), independent of the term.

$\Delta \mathcal{E}_0$ corrections	
$ \begin{aligned} &\overbrace{(n_a \ell_a) j_a^{2j_a+1} (n_b \ell_b) j_b^{2j_b+1}}^{\text{core subshells}} \overbrace{(n_m \ell_m) j_m^{w_m} (n_n \ell_n) j_n^{w_n}}^{\text{valence subshells}} \rightarrow \overbrace{(n_a \ell_a) j_a^{2j_a} (n_b \ell_b) j_b^{2j_b}}^{\text{core subshells}} \overbrace{(n_m \ell_m) j_m^{w_m} (n_n \ell_n) j_n^{w_n}}^{\text{valence subshells}} \overbrace{(n_r \ell_r) j_r (n_s \ell_s) j_s}^{\text{virtual subshells}} \\ &- \underbrace{\sqrt{[j_a]} \left[\sqrt{[j_r]} \mathcal{A}(0, ab, sr) + \sqrt{[j_s]} \mathcal{A}(0, ab, rs) \right]}_{\text{from CC}_1 \text{ Feynman diagram}} \underbrace{(-1)^{j_a+j_b+j_r+j_s} \sum_k [\mathcal{C}(k, ab, rs) + \mathcal{C}(k, ba, rs)]}_{\text{from CC}_2 \text{ Feynman diagram}} \end{aligned} $	
$ \begin{aligned} &\overbrace{(n_a \ell_a) j_a^{2j_a+1} (n_b \ell_b) j_b^{2j_b+1}}^{\text{core subshells}} \overbrace{(n_m \ell_m) j_m^{w_m} (n_n \ell_n) j_n^{w_n}}^{\text{valence subshells}} \rightarrow \overbrace{(n_a \ell_a) j_a^{2j_a} (n_b \ell_b) j_b^{2j_b}}^{\text{core subshells}} \overbrace{(n_m \ell_m) j_m^{w_m+1} (n_n \ell_n) j_n^{w_n}}^{\text{valence subshells}} \overbrace{(n_r \ell_r) j_r}^{\text{virtual subshells}} \\ &\frac{w_m - [j_m]}{[j_m]} \left\{ \underbrace{\sqrt{[j_m]} \left[\sqrt{[j_a]} \mathcal{A}(0, ab, rm) + \sqrt{[j_b]} \mathcal{A}(0, ba, rm) \right]}_{\text{from CC}_3 \text{ Feynman diagram}} \right. \\ &\left. + \underbrace{(-1)^{j_a+j_b+j_r+j_m} \sum_k [\mathcal{C}(k, ab, rm) + \mathcal{C}(k, ba, rm)]}_{\text{from CC}_4 \text{ Feynman diagram}} \right\} \end{aligned} $	

to the expressions of Feynman diagrams (see, for example, Fig. 1, Eqs. (29), (30)).

As we can see, the expression of the second type of core–core correlations (see Table 1), unlike the first type of core–core correlations, depends on the occupation number w_m of subshell m (number of electrons in the subshell m). This is due to the fact that the second type of core–core correlations is described by the CC_3 and CC_4 Feynman diagrams, the angular part of which is expressed via the operator \hat{N} of subshell occupation number (see Eq. (10)). Meanwhile, the first type of core–core correlations is described by vacuum Feynman diagrams CC_1 and CC_2 , which do not have any tensorial part in their expressions (see Subsection 2.1).

The contribution of the last two types of CC correlations in the second-order of the perturbation theory is expressed over $\Delta\mathcal{E}_0(KJ)$, $\Delta\mathcal{F}^k(n\ell j, n\ell j)$, $\Delta\mathcal{F}^k(n\ell j, n'\ell' j')$ and $\Delta\mathcal{G}^k(n\ell j, n'\ell' j')$ (see Tables 2 and 3). These formulae are additionally expressed via the quantities

$$\begin{aligned} \mathcal{A}'(x, ij, i'j') &= \\ &= \sum_{k,k'} \left\{ \begin{matrix} k & k' & x \\ j_j & j_i & j_{i'} \end{matrix} \right\} \left\{ \begin{matrix} k & k' & x \\ j_j & j_j & j_{j'} \end{matrix} \right\} \mathcal{P}(kk', ij, i'j'), \end{aligned} \quad (32)$$

$$\begin{aligned} \mathcal{B}(x, ij, i'j') &= \\ &= \sum_{k,k'} \left\{ \begin{matrix} k & k' & x \\ j_j & j_i & j_{i'} \end{matrix} \right\} \left\{ \begin{matrix} k & k' & x \\ j_i & j_j & j_{j'} \end{matrix} \right\} Q(kk', ij, i'j'). \end{aligned} \quad (33)$$

As we can see, the expression of the last two types of core–core correlations (see Table 2) for the contribution $\Delta\mathcal{E}_0$ depends on different combinations $\frac{[j]-w}{\sqrt{[j]}}$ of the subshells m and n . This is due to the fact that these types of core–core correlations are described by the CC_5 and CC_6 Feynman diagrams, the angular part of which is expressed via the combination $\frac{[j]-\hat{N}}{\sqrt{[j]}}$ of the operator acting on the n and/or m subshell (see Subsections 2.3, 2.4).

The contribution of CC correlation in the second order of the perturbation theory coming from the off-diagonal matrix element $\langle (n_m \ell_m) j_m^{w_m} (n_n \ell_n) j_n^{w_n} || \hat{\mathcal{H}}_{\text{Effective}}^{(2)} || (n_m \ell_m) j_m^{w_m-2} (n_n \ell_n) j_n^{w_n+2} \rangle$ is described by the diagram CC_6 . Reformulation of the expressions of this diagram into the form suitable for the GRASP gave these corrections only to the radial integral $\Delta\mathcal{R}^k(mm, nn)$ (see Table 4). This formula is expressed via the quantity

Table 2. Expressions for the third (where $a \neq b$ or $a = b$) and fourth (where $a \neq b$ or $a = b$) types of core–core corrections to the energy in Eq. (24), independent of the term.

$\Delta\mathcal{E}_0$ corrections	
$\overbrace{(n_a \ell_a) j_a^{2j_a+1} (n_b \ell_b) j_b^{2j_b+1}}^{\text{core subshells}} \overbrace{(n_m \ell_m) j_m^{w_m} (n_n \ell_n) j_n^{w_n}}^{\text{valence subshells}} \rightarrow \overbrace{(n_a \ell_a) j_a^{2j_a} (n_b \ell_b) j_b^{2j_b}}^{\text{core subshells}} \overbrace{(n_m \ell_m) j_m^{w_m+2} (n_n \ell_n) j_n^{w_n}}^{\text{valence subshells}}$	
$-2 \frac{([j_m]-w_m)([j_m]-w_m-1)}{[j_m]} \mathcal{A}'(0, mm, ab) + 2 \frac{[j_m]-2w_m}{[j_m]} \sum_{k>0} (-1)^k [k] \mathcal{A}'(k, mm, ab)$	from CC_5 and CC_6 Feynman diagrams
$\overbrace{(n_a \ell_a) j_a^{2j_a+1} (n_b \ell_b) j_b^{2j_b+1}}^{\text{core subshells}} \overbrace{(n_m \ell_m) j_m^{w_m} (n_n \ell_n) j_n^{w_n}}^{\text{valence subshells}} \rightarrow \overbrace{(n_a \ell_a) j_a^{2j_a} (n_b \ell_b) j_b^{2j_b}}^{\text{core subshells}} \overbrace{(n_m \ell_m) j_m^{w_m+1} (n_n \ell_n) j_n^{w_n+1}}^{\text{valence subshells}}$	
$\frac{([j_m]-w_m)([j_n]-w_n)}{\sqrt{[j_m, j_n]}} (\mathcal{A}'(0, mn, ab) + \mathcal{A}'(0, mn, ba))$	from CC_5 and CC_6 Feynman diagrams
$-\frac{(-1)^{j_m+j_n+j_a+j_b}}{2} \left(\frac{([j_m]-2w_m)}{[j_m]} + \frac{([j_n]-2w_n)}{[j_n]} \right) \sum_k (\mathcal{C}(k, ab, mn) + \mathcal{C}(k, ab, nm))$	from CC_5 and CC_6 Feynman diagrams

Table 3. Expressions for Slater integrals $\Delta\mathcal{F}^k(m, m)$, $\Delta\mathcal{F}^k(m, n)$ and $\Delta\mathcal{G}^k(m, n)$ (see Eq. (24)) corresponding to the third type $(n_a \ell_a) j_a^{2j_a+1} (n_b \ell_b) j_b^{2j_b+1} (n_m \ell_m) j_m^{w_m} (n_n \ell_n) j_n^{w_n} \rightarrow (n_a \ell_a) j_a^{2j_a} (n_b \ell_b) j_b^{2j_b} (n_m \ell_m) j_m^{w_m+2} (n_n \ell_n) j_n^{w_n}$ (where $a \neq b$ or $a = b$) and the fourth type $(n_a \ell_a) j_a^{2j_a+1} (n_b \ell_b) j_b^{2j_b+1} (n_m \ell_m) j_m^{w_m} (n_n \ell_n) j_n^{w_n} \rightarrow (n_a \ell_a) j_a^{2j_a} (n_b \ell_b) j_b^{2j_b} (n_m \ell_m) j_m^{w_m+1} (n_n \ell_n) j_n^{w_n+1}$ (where $a \neq b$ or $a = b$) of core–core correlations.

Corrections	Slater integral	k values
$\underbrace{(n_a \ell_a) j_a^{2j_a+1} (n_b \ell_b) j_b^{2j_b+1}}_{\text{core subshells}} \underbrace{(n_m \ell_m) j_m^{w_m} (n_n \ell_n) j_n^{w_n}}_{\text{valence subshells}} \rightarrow \underbrace{(n_a \ell_a) j_a^{2j_a} (n_b \ell_b) j_b^{2j_b}}_{\text{core subshells}} \underbrace{(n_m \ell_m) j_m^{w_m+2} (n_n \ell_n) j_n^{w_n}}_{\text{valence subshells}}$ $\underbrace{-4[k]\mathcal{A}'(k, mm, ab)}_{\text{from CC}_6 \text{ Feynman diagram}}$	$\Delta\mathcal{F}^k(m, m)$	$k > 0$
$\underbrace{(n_a \ell_a) j_a^{2j_a+1} (n_b \ell_b) j_b^{2j_b+1}}_{\text{core subshells}} \underbrace{(n_m \ell_m) j_m^{w_m} (n_n \ell_n) j_n^{w_n}}_{\text{valence subshells}} \rightarrow \underbrace{(n_a \ell_a) j_a^{2j_a} (n_b \ell_b) j_b^{2j_b}}_{\text{core subshells}} \underbrace{(n_m \ell_m) j_m^{w_m+1} (n_n \ell_n) j_n^{w_n+1}}_{\text{valence subshells}}$ $\underbrace{-[k](\mathcal{A}'(k, mn, ab) + \mathcal{A}'(k, mn, ba))}_{\text{from CC}_6 \text{ Feynman diagram}}$	$\Delta\mathcal{F}^k(m, n)$	$k > 0$
$\underbrace{-2[k]\mathcal{B}(k, mn, ab)}_{\text{from CC}_6 \text{ Feynman diagram}}$	$\Delta\mathcal{G}^k(m, n)$	$k \geq 0$

Table 4. Expressions for the Slater integral $\Delta\mathcal{R}^k(mm, nn)$ (see Eq. (24)) corresponding to the core–core $(n_a \ell_a) j_a^{2j_a+1} (n_b \ell_b) j_b^{2j_b+1} (n_m \ell_m) j_m^{w_m} (n_n \ell_n) j_n^{w_n} \rightarrow (n_a \ell_a) j_a^{2j_a} (n_b \ell_b) j_b^{2j_b} (n_m \ell_m) j_m^{w_m} (n_n \ell_n) j_n^{w_n+2}$ correlations coming from the off-diagonal matrix element $\langle (n_m \ell_m) j_m^{w_m} (n_n \ell_n) j_n^{w_n} | \hat{\mathcal{H}}_{\text{Effective}}^{(2)} | (n_m \ell_m) j_m^{w_m-2} (n_n \ell_n) j_n^{w_n+2} \rangle$.

Corrections	Slater integral	k values
$\underbrace{-4[k]\mathcal{X}(k, nn, ab, mm)}_{\text{from CC}_6 \text{ Feynman diagram}}$	$\Delta\mathcal{R}^k(mm, nn)$	$k \geq 0$

$$\begin{aligned} \mathcal{X}(x, ij, i'j', i''j'') &= \\ &= \sum_{k, k'} \begin{Bmatrix} k & k' & x \\ j_i & j_j & j_i j_j \end{Bmatrix} \begin{Bmatrix} k & k' & x \\ j_{i'} & j_{j'} & j_{i'} j_{j'} \end{Bmatrix} \mathcal{S}'(kk', ij, i'j', i''j''), \end{aligned} \quad (34)$$

where

$$\begin{aligned} \mathcal{S}'(kk', ij, i'j', i''j'') &= \\ &= \mathcal{R}^k(ij, i'j') \mathcal{R}^{k'}(i'j', i''j'') \mathcal{O}(K', K_1 K_2) \end{aligned} \quad (35)$$

and

$$\begin{aligned} \mathcal{O}(K', K_1 K_2) &= \\ &= \frac{1}{2} \left(\frac{1}{\bar{E}(K') - \bar{E}(K_1)} + \frac{1}{\bar{E}(K') - \bar{E}(K_2)} \right), \end{aligned} \quad (36)$$

where $\bar{E}(K_1)$ corresponds to the averaged energy of the configuration K_1 from the bra function of off-diagonal matrix element and $\bar{E}(K_2)$ corresponds to the averaged energy of the configuration K_1 from

the ket function of off-diagonal matrix element. For details on how to find them, see Ref. [1], Section 3.

This theory in an irreducible tensorial form is more suitable to be included in such version of the GRASP which is based on configuration state function generators (CSFGs) [16]. This is related to the fact that this version of the package allows us to distinguish the F , F' and G sets of orbitals very easily in the process of computing atomic data. In the following section, we will present a test case of this implementation.

4. Calculation of core–valence, core and core–core correlations with a new approach

The method, which is based on the Rayleigh–Schrödinger perturbation theory in an irreducible tensorial form [1, 2], has now been extended to

include CC correlations. In this work, the RSMBPT method is used to include CV, C and CC correlations for the calculation of the Fe XV energy structure and E1 transition properties. The energy levels of the $3s^2$, $3p^2$, $3s3d$, $3d^2$, $3p3d$, $3s3p$ configurations and the E1 transition properties between the states of these configurations are computed. The results are compared with those obtained by the regular RCI in the GRASP [17]. The radial wave functions are taken from the earlier study [2] where the computational scheme is described in detail. The RCI calculations are performed, including the Coulomb and Breit interactions and leading quantum electrodynamic effects – the vacuum polarization and self-energy corrections. Meanwhile, the estimation of correlations was done using the stationary second-order Rayleigh–Schrödinger many-body perturbation theory in an irreducible tensorial form for the Coulomb interaction.

Regular RCI results are marked as **RCI** with the correlations, which were included in the calculations, e.g. valence–valence (VV) (**VV RCI**). In this computational scheme, single–double (SD) substitutions are allowed from the $3s$, $3p_{-}$, $3p$, $3d_{-}$, $3d$ valence orbitals to the orbital set (OS) OS_1, \dots, OS_5 (see Ref. [2]). In the **VV+CV+C RCI** computational scheme, SD substitutions are allowed from the $3s$, $3p_{-}$, $3p$, $3d_{-}$, $3d$ valence orbitals and single (S) substitutions are allowed only from the $2s$ or $2p_{-}$ and $2p$ core orbital to the orbital set OS_1, \dots, OS_5 . In the **VV+CV+C+CC RCI** computational scheme, SD substitutions are allowed from the $3s$, $3p_{-}$, $3p$, $3d_{-}$, $3d$ valence orbitals and from the $2s$, $2p_{-}$ and $2p$ core orbitals to the orbital set OS_1, \dots, OS_5 . The multi-reference (MR) set consists of the $3s^2$, $3p^2$, $3s3d$, $3d^2$ even and $3p3d$, $3s3p$ odd configurations. The strategies marked as ‘int’ mean that only CSFs that have non-zero matrix elements in the sets of spin-angular integration with the CSFs belonging to the configurations in the MR are retained.

The CSF space in RSMBPT computations is divided into three sets: F , F' and G (see Ref. [1] for details). Thus, the $1s$ is defined as an inactive core subshell, $2s$, $2p_{-}$ and $2p$ subshells are defined as active core subshells (that correspond to F set), $3s$, $3p_{-}$, $3p$, $3d_{-}$, and $3d$ as valence subshells (that correspond to F' set), and subshells belonging to OS_1, \dots, OS_5 as virtual ones (that correspond

to G set). This distribution of space is consistent with regular GRASP2018 calculations and allows the use of a combination of RCI and RSMBPT methods. The results including CV, C and CC correlations according to the RSMBPT method are marked as **CV+C+CC RCI (RSMBPT)**. In this case, the contribution of each K' configuration of the CV, C and CC correlations for CSF for which energy needs to be calculated according to the Rayleigh–Schrödinger perturbation theory in an irreducible tensorial form according to Eq. (22) of Ref. [1], Eq. (6) of Ref. [2] and Eq. (26) is computed. The total contribution of the CV, C and CC correlations is also computed. K' configurations are sorted in a descending order according to the impact of the CV, C and CC correlations for each level.

Further, K' configurations are selected by the impact of CV, C and CC correlations with a specified fraction (expressed in the percentage: 95, 99, 99.5, 99.95 and 100%) of the total CV, C and CC contribution, and RCI computations are performed including them. These CSFs bases are also reduced by removing from the list the CSFs that have zero spin-angular coefficients for matrix elements with the CSFs belonging to the configurations in the MR set. Later, RCI computations are performed for the reduced CSFs base. These results are marked as ‘int’ in the further description. Note that the program gives the contribution of the CV, C and CC correlations of K' configuration with a value greater than $1.0E-11$, smaller contributions are neglected. The C and CV correlations (Eqs. (3, 4) of Ref. [2]), which are not included in the RSMBPT method, were added to RCI calculations in a regular way, together with the valence and valence–valence correlations.

4.1. Calculations of the energy structure

Table 5 presents the comparison for 35 energy levels from regular GRASP2018 calculations with NIST ASD (Atomic Structure Database) [18]. In the regular GRASP2018 calculations, VV, CV, C and CC electron correlations are included. The number of CSFs (N_{CSFs}) from each calculation and the root-mean-square (rms) with NIST data are given in the last lines of the table. It is seen from the table that the CV and C correlations are important,

Table 5. The energy levels (in cm^{-1}) and differences (in cm^{-1}) between **RCI** and **NIST** energies ($\Delta E_{(\text{RCI})-(\text{NIST})}$) for Fe XV are given when computations are performed in a regular way including VV, CV, C and CC correlations.

No.	State	NIST	$\Delta E(\text{RCI})-(\text{NIST})$				
			VV	VV+CV+C int	VV+CV+C	VV+CV+C+CC int	VV+CV+C+CC
1	$3s^2 \ ^1S_0$	0					
2	$3s3p \ ^3P_0^o$	233842	-746.91	8.17	7.82	-296.32	-301.68
3	$3s3p \ ^3P_1^o$	239660	-717.57	27.93	27.91	-285.97	-284.90
4	$3s3p \ ^3P_2^o$	253820	-798.57	23.34	23.28	-306.04	-303.93
5	$3s3p \ ^1P_1^o$	351911	2925.87	211.45	211.19	-8.53	-12.67
6	$3p^2 \ ^3P_0$	554524	1959.20	156.46	156.46	450.57	444.78
7	$3p^2 \ ^1D_2$	559600	286.67	295.66	295.62	342.25	341.33
8	$3p^2 \ ^3P_1$	564602	1840.29	121.10	121.05	401.73	394.75
9	$3p^2 \ ^3P_2$	581803	1442.72	173.83	173.81	375.78	373.70
10	$3p^2 \ ^1S_0$	659627	3045.02	511.51	511.51	715.39	703.60
11	$3s3d \ ^3D_1$	678772	1684.31	331.01	329.60	68.52	52.91
12	$3s3d \ ^3D_2$	679785	1672.03	350.25	349.51	81.77	73.14
13	$3s3d \ ^3D_3$	681416	1606.31	344.63	343.41	84.60	75.61
14	$3s3d \ ^1D_2$	762093	4112.22	547.93	545.30	673.85	647.50
15	$3p3d \ ^3F_2^o$	928241	876.83	485.29	485.01	-125.90	-126.07
16	$3p3d \ ^3F_3^o$	938126	722.00	503.29	502.30	-114.13	-113.47
17	$3p3d \ ^1D_2^o$	948513	1621.09	408.50	408.06	-176.90	-176.70
18	$3p3d \ ^3F_4^o$	949658	609.19	493.11	489.87	-135.80	-139.09
19	$3p3d \ ^3D_1^o$	982868	3141.47	349.41	348.96	-114.34	-120.13
20	$3p3d \ ^3P_2^o$	983514	2811.54	399.78	398.42	-94.87	-99.81
21	$3p3d \ ^3D_3^o$	994852	3254.23	381.16	379.36	-81.04	-85.84
22	$3p3d \ ^3P_0^o$	995889	2550.57	467.52	461.29	-58.85	-78.33
23	$3p3d \ ^3P_1^o$	996243	2747.52	439.25	438.84	-78.90	-83.97
24	$3p3d \ ^3D_2^o$	996623	2939.80	408.62	407.89	-91.96	-94.83
25	$3p3d \ ^1F_3^o$	1062515	4046.73	783.97	776.35	666.63	650.87
26	$3p3d \ ^1P_1^o$	1074887	3603.75	944.60	941.74	728.85	701.36
27	$3d^2 \ ^3F_2$	1370331	2834.22	795.74	795.41	159.05	151.58
28	$3d^2 \ ^3F_3$	1372035	2752.53	776.22	775.43	148.44	139.34
29	$3d^2 \ ^3F_4$	1374056	2713.16	804.78	804.19	176.26	171.07
30	$3d^2 \ ^1D_2$	1402592	2813.26	1079.22	1077.95	458.53	442.70
31	$3d^2 \ ^3P_0$						
32	$3d^2 \ ^3P_1$						
33	$3d^2 \ ^1G_4$	1407058	2385.95	1141.81	1139.46	737.52	726.46
34	$3d^2 \ ^3P_2$	1407773	3038.87	932.00	931.75	195.23	187.31
35	$3d^2 \ ^1S_0$	1487054	2379.42	1975.89	1975.89	1143.47	1120.02
N_{CSFs}			4485	372043	430629	2241061	5864226
rms (in cm^{-1})			2438.25	653.16	652.01	401.16	392.76

the rms deviation obtained for the energy levels from the NIST data is 653.16 cm^{-1} . By including CC correlations the rms deviation decreases to 401.16 cm^{-1} .

Table 6 shows the total energies from regular GRASP2018 calculations (**VV+CV+C+CC RCI int**) for 35 computed states. These energies are computed after the CSF base reduction

Table 6. The total energies (in a.u.) from the **VV+CV+C+CC RCI int** calculations and differences (in a.u.) between the **VV+CV+C+CC RCI** energies and **VV+CV+C+CC RCI int** energies ($\Delta E_{(\text{RCI})-(\text{RCI int})} \equiv \Delta E_{(\text{VV+CV+C+CC RCI})-(\text{VV+CV+C+CC RCI int})}$) and differences (in a.u.) between **CV+C+CC RCI (RSMBPT)** and **VV+CV+C+CC RCI int** energies ($\Delta E_{(\text{RCI (RSMBPT)})-(\text{RCI int})} \equiv \Delta E_{(\text{CV+C+CC RCI (RSMBPT)})-(\text{VV+CV+C+CC RCI int})}$) for Fe XV are given when CV, C and CC correlations are included in the computations.

No.	State	VV+CV+C+CC RCI		$\Delta E_{(\text{RCI (RSMBPT)})-(\text{RCI int})}$	
		int	$\Delta E_{(\text{RCI})-(\text{RCI int})}$	100% int	100%
1	3s ² ¹ S ₀	-1182.73096327	-0.00003815	0.00000009	-0.00001565
2	3s3p ³ P ₀	-1181.66685085	-0.00006259	0.00000051	-0.00001094
3	3s3p ³ P ₁	-1181.64029495	-0.00003326	0.00000046	-0.00001510
4	3s3p ³ P ₂	-1181.57586867	-0.00002856	0.00000019	-0.00001482
5	3s3p ¹ P ₁	-1181.12757765	-0.00005702	0.00000065	-0.00003104
6	3p ² ³ P ₀	-1180.20231307	-0.00006452	0.00000010	-0.00001675
7	3p ² ¹ D ₂	-1180.17967864	-0.00004235	0.00000035	-0.00002700
8	3p ² ³ P ₁	-1180.15661687	-0.00006994	0.00000018	-0.00001747
9	3p ² ³ P ₂	-1180.07836156	-0.00004763	0.00000015	-0.00003757
10	3p ² ¹ S ₀	-1179.72222197	-0.00009184	0.00000008	-0.00004238
11	3s3d ³ D ₁	-1179.63793828	-0.00010929	0.00000111	-0.00002709
12	3s3d ³ D ₂	-1179.63326232	-0.00007751	0.00000230	-0.00004417
13	3s3d ³ D ₃	-1179.62581805	-0.00007913	0.00000064	-0.00001844
14	3s3d ¹ D ₂	-1179.25554176	-0.00015821	0.00000409	-0.00008186
15	3p3d ³ F ₂	-1178.50215971	-0.00003895	0.00000326	-0.00001497
16	3p3d ³ F ₃	-1178.45706670	-0.00003518	0.00000132	-0.00001109
17	3p3d ¹ D ₂	-1178.41002605	-0.00003725	0.00000086	-0.00001810
18	3p3d ³ F ₄	-1178.40462181	-0.00005311	0.00000020	-0.00000916
19	3p3d ³ D ₁	-1178.25320812	-0.00006454	0.00000245	-0.00002416
20	3p3d ³ P ₂	-1178.25017600	-0.00006067	0.00000054	-0.00002796
21	3p3d ³ D ₃	-1178.19845329	-0.00006000	0.00000102	-0.00002579
22	3p3d ³ P ₀	-1178.19362723	-0.00012693	0.00000128	-0.00002239
23	3p3d ³ P ₁	-1178.19210564	-0.00006127	0.00000281	-0.00003106
24	3p3d ³ D ₂	-1178.19043378	-0.00005120	0.00000183	-0.00002695
25	3p3d ¹ F ₃	-1177.88675130	-0.00010997	0.00000806	-0.00003279
26	3p3d ¹ P ₁	-1177.83009684	-0.00016344	0.00000423	-0.00006022
27	3d ² ³ F ₂	-1176.48655116	-0.00007218	0.00000319	-0.00004057
28	3d ² ³ F ₃	-1176.47883548	-0.00007960	0.00000059	-0.00001869
29	3d ² ³ F ₄	-1176.46950039	-0.00006180	0.00000028	-0.00003522
30	3d ² ¹ D ₂	-1176.33819466	-0.00011029	0.00000238	-0.00005909
31	3d ² ³ P ₀	-1176.32567236	-0.00009761	0.00000009	-0.00003160
32	3d ² ³ P ₁	-1176.32276134	-0.00009015	0.00000057	-0.00002843
33	3d ² ¹ G ₄	-1176.31657493	-0.00008852	0.00000109	-0.00004105
34	3d ² ³ P ₂	-1176.31578797	-0.00007427	0.00000043	-0.00004825
35	3d ² ¹ S ₀	-1175.95023666	-0.00014501	0.00000009	-0.00006050
	N_{CSFs}	2241061	5864226	2166376	3033360

mentioned in the previous section. Next to this column are the differences of the total energies from the **VV+CV+C+CC RCI** computations, which

are obtained before a base reduction. The changes in total energies are small when reduction is applied, but the size of the CSF base decreases more

than twice. In the same Table, the energy differences between the **CV+C+CC RCI (RSMBPT)** when 100% of CV, C, CC correlations are included, and regular **VV+CV+C+CC RCI int** results ($\Delta E_{(CV+C+CC \text{ RCI (RSMBPT)})-(VV+CV+C+CC \text{ RCI int})}$) are given. This comparison shows that the total energies using the RSMBPT method (with a reduction column 100% int and without a reduction column 100%) reproduce the regular GRASP2018 results. In the case of ‘int’, we have the negligible difference (to 8.0E-06 a.u. or 0.0000000068%) which could be due to omitted CV, C and CC correlations with a very small contribution (1.0E-11).

In Table 7, the energy levels from the regular GRASP2018 calculations **VV+CV+C+CC RCI** and from the calculations using the RSMBPT method (**CV+C+CC RCI (RSMBPT)**) are compared. The calculations using the RSMBPT method are carried out in five steps, including 95, 99, 99.5, 99.95 and 100% of CV, C and CC correlations. In the last line of the table, the root-mean-square (rms) with the results of regular GRASP2018 calculations (**VV+CV+C+CC RCI int**) are given. By adding the most important K' configurations of CV, C and CC correlations step by step, the results converge to the results of regular GRASP2018 calculations and, in the case of ‘100% int’, are in an excellent agreement with them. The difference in this case is only up to 2 cm⁻¹, which may be due to the omission of CV, C and CC correlations with a contribution less than 1.0E-11 (as mentioned in the discussion of Table 6). When CSFs with a smaller impact of the CV, C and CC correlations are omitted, the energy levels are similar to these from the regular computations. For example, if 99% (case 99% int) of the CV, C and CC correlations are included in the computations, the rms with **VV+CV+C+CC RCI int** results is 68.93 cm⁻¹, and the largest difference between the results of these calculations is only up to 200 cm⁻¹. Meanwhile, the space of CSFs decreases almost twice comparing to the space in the **VV+CV+C+CC RCI int** computations.

4.2. Calculation of E1 transition properties

We computed the transition properties of E1 transitions between the abovementioned levels. The calculations are done in a regular way by including different types of correlations and using

the RSMBPT method. Below we present a comparison of the line strengths using different computational schemes (Table 8 and Figs. 7, 8). We also give the statistics for all computed transitions (Figs. 9, 10). The uncertainties of the line strengths obtained in this work are estimated based on the quantitative and qualitative evaluation (QQE) method described in Refs. [19, 20].

Table 8 shows the comparison of the line strengths, cancellation factors (CF) [21], the $G_{S=0}$ parameters [19, 20], and the estimated accuracy for few strongest and for few weaker E1 transitions using different computational schemes. The Table also includes lines for each transition marked with ‘NIST’ as these data are critically evaluated by the NIST [18]. These lines contain the observed wavelength and line strength with the critically evaluated accuracy. As seen from the Table, using the regular computational scheme, the CV and C correlations have the largest impact on the line strengths, adding the CC correlations the line strengths change a little. By using the RSMBPT method it is seen that by including the most important K' configurations of CV, C and CC correlations, the line strengths agree with the regular GRASP2018 calculations when CV, C and CC correlations are included. Excluding the CV, C, CC correlations with the smallest impact (cases 99.95, 99.5, 99 and 95% in Table 8), we see that the line strength almost does not change compared to the results when all these correlations are included. From Table 8 we also see that the CFs in both (Babushkin and Coulomb) gauges change when a new group of correlations is added to the regular GRASP2018 calculations. Using the RSMBPT method, the values of CF are stable when the most important configurations of CV, C and CC correlations in a different amount are included and the configurations of CV, C and CC correlations with the smallest impact are neglected. The change in the values of CFs indicates the importance of added correlations in the calculations. By using a regular method for inclusion of a new group of correlations we can have such cases (as the last transition in Table 8) when the values of line strength from two computational strategies disagree more than the accuracy class assigned to transition. This situation was observed for some transitions assigned to the best accuracy classes. For example, the line strength of the 3s3p

Table 7. The energy levels (in cm^{-1}) and differences (in cm^{-1}) between the **CV+C+CC RCI (RSMBPT)** and **VV+CV+C+CC RCI int** energies ($\Delta E_{(\text{CV+C+CC RCI (RSMBPT)})-(\text{VV+CV+C+CC RCI int})}$) for Fe XV are given when CV, C and CC correlations are included in the computations.

No.	State	VV+CV+C+CC RCI		$\Delta E_{(\text{CV+C+CC RCI (RSMBPT)})-(\text{VV+CV+C+CC RCI int})}$										
			int	95%	95% int	99%	99% int	99.5%	99.5% int	99.95%	99.95% int	100%	100% int	
1	$3s^2 \ ^1S_0$	0.00	0.00											
2	$3s3p \ ^3P_0^o$	233540.32	233545.68	269.24	268.63	98.71	97.70	86.10	85.17	28.91	28.03	1.04	0.09	
3	$3s3p \ ^3P_1^o$	239375.10	239374.03	26.84	26.50	-7.13	-7.51	3.96	3.70	1.67	1.67	0.12	0.08	
4	$3s3p \ ^3P_2^o$	253516.07	253513.96	107.85	107.63	30.50	30.16	19.82	19.50	6.30	6.19	0.18	0.02	
5	$3s3p \ ^1P_1^o$	351898.33	351902.47	-27.93	-25.84	-28.78	-26.15	-15.29	-12.44	-3.59	-0.11	-3.38	0.12	
6	$3p^2 \ ^3P_0$	554968.78	554974.57	95.62	95.68	22.36	22.31	24.60	24.59	11.46	11.55	-0.24	0.00	
7	$3p^2 \ ^1D_2$	559941.33	559942.25	-20.74	-19.25	-27.95	-26.27	-31.06	-29.26	-11.44	-9.34	-2.49	0.06	
8	$3p^2 \ ^3P_1$	564996.75	565003.73	138.27	138.53	42.76	42.84	18.54	18.66	4.03	4.28	-0.40	0.02	
9	$3p^2 \ ^3P_2$	582176.70	582178.78	-66.36	-62.91	-73.46	-69.68	-58.10	-54.15	-15.52	-11.27	-4.81	0.02	
10	$3p^2 \ ^1S_0$	660330.60	660342.39	65.22	69.98	7.13	12.31	1.12	6.44	0.21	5.72	-5.87	0.00	
11	$3s3d \ ^3D_1$	678824.91	678840.52	67.36	68.47	27.54	29.14	-1.80	-0.05	-5.67	-3.55	-2.51	0.22	
12	$3s3d \ ^3D_2$	679858.14	679866.77	-149.64	-146.78	-64.98	-61.02	-49.64	-45.30	-23.87	-18.62	-6.26	0.49	
13	$3s3d \ ^3D_3$	681491.61	681500.60	130.96	130.78	36.85	36.83	23.13	23.19	-9.37	-8.87	-0.61	0.12	
14	$3s3d \ ^1D_2$	762740.50	762766.85	-111.94	-105.07	-65.59	-55.96	-52.66	-42.20	-27.10	-14.63	-14.53	0.88	
15	$3p3d \ ^3F_2^o$	928114.93	928115.10	113.06	112.34	56.94	56.38	39.81	39.68	4.38	4.85	0.15	0.70	
16	$3p3d \ ^3F_3^o$	938012.53	938011.87	326.85	325.85	109.11	108.03	67.58	66.59	13.83	13.08	1.01	0.27	
17	$3p3d \ ^1D_2^o$	948336.30	948336.10	70.58	70.43	15.00	14.99	3.96	4.13	-3.70	-3.08	-0.53	0.17	
18	$3p3d \ ^3F_4^o$	949518.91	949522.20	491.20	489.86	184.61	183.15	109.42	107.98	21.67	20.32	1.42	0.02	
19	$3p3d \ ^3D_1^o$	982747.87	982753.66	167.53	167.81	35.77	36.50	28.10	29.35	0.41	2.38	-1.87	0.52	
20	$3p3d \ ^3P_2^o$	983414.19	983419.13	93.92	94.79	26.46	27.94	10.51	12.16	-3.24	-0.81	-2.70	0.11	
21	$3p3d \ ^3D_3^o$	994766.16	994770.96	227.51	228.31	80.34	81.70	51.84	53.48	3.12	5.37	-2.23	0.20	
22	$3p3d \ ^3P_0^o$	995810.67	995830.15	357.05	358.06	190.21	191.71	105.13	106.82	27.32	29.11	-1.47	0.27	
23	$3p3d \ ^3P_1^o$	996159.03	996164.10	83.70	84.84	-2.46	-0.44	-5.12	-2.19	-6.24	-2.48	-3.38	0.60	
24	$3p3d \ ^3D_2^o$	996528.17	996531.04	10.93	11.81	-4.60	-3.05	-6.93	-5.06	-7.33	-4.61	-2.48	0.38	
25	$3p3d \ ^1F_3^o$	1063165.87	1063181.63	250.48	252.57	93.45	96.76	61.00	64.93	6.67	11.86	-3.75	1.76	
26	$3p3d \ ^1P_1^o$	1075588.36	1075615.85	114.33	117.36	36.38	42.97	16.88	24.45	-8.23	1.69	-9.78	0.91	
27	$3d^2 \ ^3F_2$	1370482.58	1370490.05	-144.36	-142.48	-70.01	-66.81	-52.54	-48.78	-23.73	-19.12	-5.47	0.68	
28	$3d^2 \ ^3F_3$	1372174.34	1372183.44	217.40	217.20	52.82	52.80	25.63	25.74	-5.82	-5.50	-0.66	0.11	
29	$3d^2 \ ^3F_4$	1374227.07	1374232.26	121.04	122.80	7.66	10.51	-19.51	-16.53	-13.99	-10.42	-4.30	0.04	
30	$3d^2 \ ^1D_2$	1403034.70	1403050.53	-209.47	-205.43	-90.09	-83.82	-68.86	-62.04	-30.38	-22.18	-9.53	0.51	
31	$3d^2 \ ^3P_0$	1405785.81	1405798.86	143.08	145.54	34.99	37.82	22.03	25.00	-0.39	2.85	-3.50	0.00	
32	$3d^2 \ ^3P_1$	1406426.34	1406437.76	171.29	173.07	40.32	42.53	8.35	10.72	-9.14	-6.58	-2.81	0.10	
33	$3d^2 \ ^1G_4$	1407784.46	1407795.52	-15.12	-10.90	38.56	40.54	10.65	12.84	-8.82	-5.68	-5.58	0.22	
34	$3d^2 \ ^3P_2$	1407960.31	1407968.23	-13.82	-13.14	-91.34	-85.61	-73.08	-67.10	-30.13	-23.50	-7.15	0.08	
35	$3d^2 \ ^1S_0$	1488174.02	1488197.47	113.10	120.88	27.43	35.89	15.96	24.61	-6.97	2.21	-9.84	0.00	
N_{CSFs}		5864226	2241061	1030900	717523	1777303	1227367	2033820	1413852	2607682	1840752	3033360	2166376	
rms (in cm^{-1})				174.40	174.39	69.49	68.93	45.63	44.70	14.69	12.35	4.91	0.46	

$^3P_1^o - 3p^2 \ ^1D_2$ transition in both (**VV+CV+C RCI int** and **VV+CV+C+CC RCI int**) strategies is assigned to the AA accuracy class. In the regular GRASP2018 calculations in the **VV+CV+C RCI int** strategy, the line strength in the Babushkin

gauge is $9.14394\text{E-}02$ a.u., meanwhile when CC correlations were added (**VV+CV+C+CC RCI int** strategy), the line strength in the Babushkin gauge is equal to $8.99187\text{E-}02$ a.u. Whereas using the RSMBPT method when the CV, C and CC

Table 8. Comparison of the computed wavelengths (λ in Å), line strengths (S in a.u.), cancellation factors, and the $G_{S=0}$ parameters using different strategies. S_B is the line strength in the Babushkin gauge, S_C is the line strength in the Coulomb gauge. The name of the computational scheme **CV+C+CC RCI(RSMBPT)** is marked as **RCI (RSMBPT)** in the Table.

Strategy	λ	S_B	S_C	CF_B	CF_C	$G_{S=0}$	Acc.
$3s\ 3p\ ^1P_1^o - 3s\ 3d\ ^1D_2$							
VV RCI	243.09	1.50687E+00	1.58586E+00	7.07E-01	7.98E-01	5.60659E+01	B+
VV+CV+C RCI int	243.59	1.43765E+00	1.43571E+00	6.59E-01	3.83E-01	-2.09378E+03	AA
VV+CV+C RCI	243.60	1.43765E+00	1.43577E+00	6.59E-01	3.83E-01	-2.15614E+03	AA
VV+CV+C+CC RCI int	243.39	1.44376E+00	1.44403E+00	6.60E-01	3.83E-01	1.48600E+04	AA
VV+CV+C+CC RCI	243.40	1.44367E+00	1.44383E+00	6.59E-01	3.82E-01	2.59365E+04	AA
RCI (RSMBPT) 100%	243.40	1.44367E+00	1.44370E+00	6.60E-01	3.82E-01	1.44867E+05	AA
RCI (RSMBPT) 100% int	243.39	1.44376E+00	1.44402E+00	6.60E-01	3.83E-01	1.55237E+04	AA
RCI (RSMBPT) 99.95%	243.40	1.44371E+00	1.44386E+00	6.60E-01	3.83E-01	2.62284E+04	AA
RCI (RSMBPT) 99.95% int	243.40	1.44380E+00	1.44420E+00	6.60E-01	3.83E-01	1.00242E+04	AA
RCI (RSMBPT) 99.5%	243.41	1.44379E+00	1.44434E+00	6.60E-01	3.83E-01	7.46809E+03	AA
RCI (RSMBPT) 99.5% int	243.41	1.44389E+00	1.44471E+00	6.60E-01	3.84E-01	4.96748E+03	AA
RCI (RSMBPT) 99%	243.41	1.44392E+00	1.44493E+00	6.60E-01	3.84E-01	4.04749E+03	AA
RCI (RSMBPT) 99% int	243.41	1.44401E+00	1.44530E+00	6.60E-01	3.85E-01	3.15843E+03	AA
RCI (RSMBPT) 95%	243.44	1.44460E+00	1.44562E+00	6.60E-01	3.88E-01	4.03134E+03	AA
RCI (RSMBPT) 95% int	243.44	1.44470E+00	1.44599E+00	6.60E-01	3.89E-01	3.16669E+03	AA
NIST [18]	243.794	1.5E+00					D
$3p^2\ ^3P_2 - 3p\ 3d\ ^3D_3^o$							
VV RCI	241.04	1.20534E+00	1.28606E+00	5.05E-01	5.42E-01	4.43456E+01	B+
VV+CV+C RCI int	241.98	1.11498E+00	1.10652E+00	4.57E-01	2.59E-01	-3.70647E+02	AA
VV+CV+C RCI	241.98	1.11499E+00	1.10653E+00	4.57E-01	2.59E-01	-3.70698E+02	AA
VV+CV+C+CC RCI int	242.37	1.12568E+00	1.12684E+00	4.60E-01	2.60E-01	2.76724E+03	AA
VV+CV+C+CC RCI	242.37	1.12551E+00	1.12672E+00	4.60E-01	2.60E-01	2.64286E+03	AA
RCI (RSMBPT) 100%	242.37	1.12557E+00	1.12677E+00	4.60E-01	2.60E-01	2.66400E+03	AA
RCI (RSMBPT) 100% int	242.37	1.12569E+00	1.12684E+00	4.60E-01	2.60E-01	2.76393E+03	AA
RCI (RSMBPT) 99.95%	242.36	1.12575E+00	1.12637E+00	4.60E-01	2.61E-01	5.16207E+03	AA
RCI (RSMBPT) 99.95% int	242.36	1.12586E+00	1.12647E+00	4.60E-01	2.61E-01	5.21141E+03	AA
RCI (RSMBPT) 99.5%	242.31	1.12621E+00	1.12583E+00	4.60E-01	2.63E-01	-8.45922E+03	AA
RCI (RSMBPT) 99.5% int	242.31	1.12631E+00	1.12595E+00	4.60E-01	2.63E-01	-8.81998E+03	AA
RCI (RSMBPT) 99%	242.28	1.12673E+00	1.12562E+00	4.60E-01	2.64E-01	-2.87810E+03	AA
RCI (RSMBPT) 99% int	242.28	1.12684E+00	1.12575E+00	4.60E-01	2.64E-01	-2.94103E+03	AA
RCI (RSMBPT) 95%	242.20	1.12779E+00	1.12878E+00	4.61E-01	2.67E-01	3.22883E+03	AA
RCI (RSMBPT) 95% int	242.20	1.12789E+00	1.12891E+00	4.61E-01	2.67E-01	3.13652E+03	AA
NIST [18]	242.100	1.1E+00					D
$3s\ 3d\ ^1D_2 - 3p\ 3d\ ^1F_3^o$							
VV RCI	332.94	2.21030E+00	2.22678E+00	7.54E-01	3.54E-01	3.81508E+02	AA
VV+CV+C RCI int	332.60	2.11114E+00	2.12236E+00	7.04E-01	1.93E-01	5.34174E+02	AA
VV+CV+C RCI	332.61	2.11102E+00	2.12186E+00	7.04E-01	1.93E-01	5.53027E+02	AA
VV+CV+C+CC RCI int	332.87	2.12945E+00	2.20008E+00	7.10E-01	2.00E-01	8.73887E+01	B+
VV+CV+C+CC RCI	332.86	2.12925E+00	2.19992E+00	7.10E-01	2.00E-01	8.73377E+01	B+
RCI (RSMBPT) 100%	332.86	2.12938E+00	2.20043E+00	7.10E-01	2.00E-01	8.68847E+01	B+

Table 8. (Continued)

Strategy	λ	S_B	S_C	CF_B	CF_C	$G_{S=0}$	Acc.
RCI (RSMBPT) 100% int	332.87	2.12948E+00	2.20021E+00	7.10E-01	2.00E-01	8.72685E+01	B+
RCI (RSMBPT) 99.95%	332.84	2.12948E+00	2.19936E+00	7.10E-01	2.00E-01	8.83069E+01	B+
RCI (RSMBPT) 99.95% int	332.84	2.12957E+00	2.19922E+00	7.10E-01	2.00E-01	8.85934E+01	B+
RCI (RSMBPT) 99.5%	332.75	2.12964E+00	2.19978E+00	7.11E-01	2.01E-01	8.79876E+01	B+
RCI (RSMBPT) 99.5% int	332.75	2.12973E+00	2.19970E+00	7.11E-01	2.01E-01	8.82038E+01	B+
RCI (RSMBPT) 99%	332.70	2.12982E+00	2.19981E+00	7.11E-01	2.01E-01	8.81840E+01	B+
RCI (RSMBPT) 99% int	332.70	2.12991E+00	2.19976E+00	7.11E-01	2.01E-01	8.83611E+01	B+
RCI (RSMBPT) 95%	332.47	2.13084E+00	2.19738E+00	7.11E-01	2.04E-01	9.26952E+01	B+
RCI (RSMBPT) 95% int	332.48	2.13093E+00	2.19740E+00	7.11E-01	2.04E-01	9.27792E+01	B+
NIST [18]	332.854	2.3E+00					D
$3s3d\ ^3D_3 - 3p\ 3d\ ^3P_4$							
VV RCI	374.19	1.30935E+00	1.26293E+00	8.84E-01	4.79E-01	-7.76641E+01	B+
VV+CV+C RCI int	372.59	1.26123E+00	1.28633E+00	8.20E-01	2.31E-01	1.44239E+02	A+
VV+CV+C RCI	372.59	1.26107E+00	1.28489E+00	8.20E-01	2.30E-01	1.51858E+02	A+
VV+CV+C+CC RCI int	373.10	1.26785E+00	1.31118E+00	8.26E-01	2.36E-01	8.48785E+01	B+
VV+CV+C+CC RCI	373.10	1.26760E+00	1.31038E+00	8.26E-01	2.35E-01	8.59229E+01	B+
RCI (RSMBPT) 100%	373.10	1.26782E+00	1.31121E+00	8.26E-01	2.36E-01	8.47539E+01	B+
RCI (RSMBPT) 100% int	373.10	1.26785E+00	1.31117E+00	8.26E-01	2.36E-01	8.49020E+01	B+
RCI (RSMBPT) 99.95%	373.06	1.26783E+00	1.31075E+00	8.26E-01	2.36E-01	8.56675E+01	B+
RCI (RSMBPT) 99.95% int	373.06	1.26786E+00	1.31071E+00	8.26E-01	2.36E-01	8.57989E+01	B+
RCI (RSMBPT) 99.5%	372.98	1.26787E+00	1.31123E+00	8.26E-01	2.37E-01	8.48162E+01	B+
RCI (RSMBPT) 99.5% int	372.99	1.26790E+00	1.31124E+00	8.27E-01	2.37E-01	8.48627E+01	B+
RCI (RSMBPT) 99%	372.90	1.26795E+00	1.31118E+00	8.27E-01	2.38E-01	8.50709E+01	B+
RCI (RSMBPT) 99% int	372.90	1.26798E+00	1.31119E+00	8.27E-01	2.38E-01	8.51050E+01	B+
RCI (RSMBPT) 95%	372.60	1.26875E+00	1.30879E+00	8.28E-01	2.45E-01	9.17442E+01	B+
RCI (RSMBPT) 95% int	372.61	1.26877E+00	1.30885E+00	8.28E-01	2.45E-01	9.16625E+01	B+
NIST [18]	372.798	1.4E+00					C
$3s3d\ ^3D_3^o - 3d^2\ ^3F_4$							
VV RCI	264.09	1.77897E+00	1.86728E+00	6.83E-01	4.99E-01	5.90906E+01	B+
VV+CV+C RCI int	263.42	1.71766E+00	1.70682E+00	6.36E-01	2.63E-01	-4.46079E+02	AA
VV+CV+C RCI	263.42	1.71761E+00	1.70689E+00	6.36E-01	2.63E-01	-4.51378E+02	AA
VV+CV+C+CC RCI int	263.53	1.72784E+00	1.73836E+00	6.41E-01	2.68E-01	4.66749E+02	AA
VV+CV+C+CC RCI	263.53	1.72755E+00	1.73736E+00	6.41E-01	2.68E-01	5.00049E+02	AA
RCI (RSMBPT) 100%	263.53	1.72767E+00	1.73759E+00	6.41E-01	2.68E-01	4.94699E+02	AA
RCI (RSMBPT) 100% int	263.53	1.72784E+00	1.73834E+00	6.41E-01	2.68E-01	4.67579E+02	AA
RCI (RSMBPT) 99.95%	263.54	1.72770E+00	1.73812E+00	6.41E-01	2.68E-01	4.71248E+02	AA
RCI (RSMBPT) 99.95% int	263.54	1.72785E+00	1.73874E+00	6.41E-01	2.68E-01	4.50894E+02	AA
RCI (RSMBPT) 99.5%	263.58	1.72787E+00	1.73975E+00	6.42E-01	2.70E-01	4.13263E+02	AA
RCI (RSMBPT) 99.5% int	263.58	1.72798E+00	1.74031E+00	6.42E-01	2.71E-01	3.98493E+02	AA
RCI (RSMBPT) 99%	263.58	1.72811E+00	1.73756E+00	6.42E-01	2.71E-01	5.19328E+02	AA
RCI (RSMBPT) 99% int	263.58	1.72822E+00	1.73814E+00	6.42E-01	2.72E-01	4.94635E+02	AA
RCI (RSMBPT) 95%	263.61	1.72863E+00	1.73934E+00	6.43E-01	2.75E-01	4.58395E+02	AA
RCI (RSMBPT) 95% int	263.60	1.72870E+00	1.73975E+00	6.43E-01	2.75E-01	4.44366E+02	AA
NIST [18]	263.685						

Table 8. (Continued)

Strategy	λ	S_B	S_C	CF_B	CF_C	$G_{S=0}$	Acc.
$3p\ 3d\ ^1F_3 - 3d^2\ ^1G_4$							
VV RCI	291.65	2.47785E+00	2.50553E+00	7.86E-01	3.61E-01	2.55295E+02	A+
VV+CV+C RCI int	289.94	2.39937E+00	2.39099E+00	7.42E-01	2.20E-01	-8.08404E+02	AA
VV+CV+C RCI	289.93	2.39926E+00	2.39116E+00	7.42E-01	2.20E-01	-8.35282E+02	AA
VV+CV+C+CC RCI int	290.18	2.41917E+00	2.47806E+00	7.51E-01	2.28E-01	1.18305E+02	A
VV+CV+C+CC RCI	290.18	2.41869E+00	2.47617E+00	7.50E-01	2.28E-01	1.21141E+02	A
RCI (RSMBPT) 100%	290.18	2.41894E+00	2.47673E+00	7.50E-01	2.28E-01	1.20497E+02	A
RCI (RSMBPT) 100% int	290.18	2.41918E+00	2.47796E+00	7.51E-01	2.28E-01	1.18529E+02	A
RCI (RSMBPT) 99.95%	290.19	2.41910E+00	2.47727E+00	7.50E-01	2.28E-01	1.19762E+02	A
RCI (RSMBPT) 99.95% int	290.19	2.41924E+00	2.47797E+00	7.51E-01	2.28E-01	1.18630E+02	A
RCI (RSMBPT) 99.5%	290.22	2.41940E+00	2.47670E+00	7.51E-01	2.30E-01	1.21529E+02	A
RCI (RSMBPT) 99.5% int	290.22	2.41950E+00	2.47729E+00	7.51E-01	2.30E-01	1.20526E+02	A
RCI (RSMBPT) 99%	290.23	2.41970E+00	2.47552E+00	7.51E-01	2.30E-01	1.24713E+02	A
RCI (RSMBPT) 99% int	290.23	2.41979E+00	2.47612E+00	7.51E-01	2.30E-01	1.23607E+02	A
RCI (RSMBPT) 95%	290.26	2.42061E+00	2.48296E+00	7.51E-01	2.32E-01	1.11922E+02	A
RCI (RSMBPT) 95% int	290.26	2.42065E+00	2.48329E+00	7.51E-01	2.32E-01	1.11417E+02	A
NIST [18]	290.239						
$3s^2\ ^1S_0 - 3s\ 3p\ ^1P_1^o$							
VV RCI	281.82	7.56430E-01	7.73811E-01	6.96E-01	9.16E-01	1.25218E+02	A
VV+CV+C RCI int	283.99	7.29184E-01	7.38054E-01	6.49E-01	3.85E-01	2.34642E+02	A+
VV+CV+C RCI	283.99	7.29185E-01	7.38056E-01	6.49E-01	3.85E-01	2.34601E+02	A+
VV+CV+C+CC RCI int	284.17	7.31169E-01	7.40656E-01	6.51E-01	3.87E-01	2.20107E+02	A+
VV+CV+C+CC RCI	284.17	7.31146E-01	7.40965E-01	6.51E-01	3.87E-01	2.12736E+02	A+
RCI (RSMBPT) 100%	284.17	7.31157E-01	7.40734E-01	6.51E-01	3.87E-01	2.18044E+02	A+
RCI (RSMBPT) 100% int	284.17	7.31169E-01	7.40655E-01	6.51E-01	3.87E-01	2.20131E+02	A+
RCI (RSMBPT) 99.95%	284.17	7.31158E-01	7.40735E-01	6.51E-01	3.87E-01	2.18053E+02	A+
RCI (RSMBPT) 99.95% int	284.17	7.31170E-01	7.40660E-01	6.51E-01	3.87E-01	2.20060E+02	A+
RCI (RSMBPT) 99.5%	284.18	7.31194E-01	7.41184E-01	6.51E-01	3.88E-01	2.09130E+02	A+
RCI (RSMBPT) 99.5% int	284.18	7.31206E-01	7.41113E-01	6.51E-01	3.88E-01	2.10878E+02	A+
RCI (RSMBPT) 99%	284.19	7.31229E-01	7.41656E-01	6.51E-01	3.89E-01	2.00463E+02	A+
RCI (RSMBPT) 99% int	284.19	7.31241E-01	7.41586E-01	6.51E-01	3.89E-01	2.02046E+02	A+
RCI (RSMBPT) 95%	284.19	7.31539E-01	7.41170E-01	6.52E-01	3.95E-01	2.16958E+02	A+
RCI (RSMBPT) 95% int	284.19	7.31549E-01	7.41128E-01	6.52E-01	3.95E-01	2.18128E+02	A+
NIST [18]	284.164	7.75E-01					B
$3s^2\ ^1S_0 - 3s\ 3p\ ^3P_1^o$							
VV RCI	418.51	4.45691E-03	4.76312E-03	4.90E-03	3.14E-03	4.32771E+01	B+
VV+CV+C RCI int	417.21	4.62691E-03	4.88159E-03	5.00E-03	1.91E-03	5.34981E+01	B+
VV+CV+C RCI	417.21	4.62689E-03	4.88153E-03	5.00E-03	1.91E-03	5.35056E+01	B+
VV+CV+C+CC RCI int	417.76	4.61939E-03	4.88880E-03	5.00E-03	1.92E-03	5.06082E+01	B+
VV+CV+C+CC RCI	417.75	4.62086E-03	4.89484E-03	5.00E-03	1.92E-03	4.98157E+01	B+
RCI (RSMBPT) 100%	417.76	4.61967E-03	4.88114E-03	5.00E-03	1.92E-03	5.20843E+01	B+
RCI (RSMBPT) 100% int	417.76	4.61935E-03	4.88875E-03	5.00E-03	1.92E-03	5.06101E+01	B+
RCI (RSMBPT) 99.95%	417.75	4.61863E-03	4.88024E-03	5.00E-03	1.92E-03	5.20462E+01	B+
RCI (RSMBPT) 99.95% int	417.75	4.61834E-03	4.88798E-03	5.00E-03	1.92E-03	5.05559E+01	B+
RCI (RSMBPT) 99.5%	417.75	4.60860E-03	4.83438E-03	4.99E-03	1.91E-03	5.98457E+01	B+

Table 8. (Continued)

Strategy	λ	S_B	S_C	CF_B	CF_C	$G_{S=0}$	Acc.
RCI (RSMBPT) 99.5% int	417.75	4.60837E-03	4.84216E-03	4.99E-03	1.91E-03	5.78640E+01	B+
RCI (RSMBPT) 99%	417.77	4.61154E-03	4.83255E-03	4.99E-03	1.91E-03	6.11318E+01	B+
RCI (RSMBPT) 99% int	417.77	4.61139E-03	4.84048E-03	4.99E-03	1.91E-03	5.90466E+01	B+
RCI (RSMBPT) 95%	417.71	4.60610E-03	4.77256E-03	4.99E-03	1.91E-03	8.03799E+01	B+
RCI (RSMBPT) 95% int	417.71	4.60598E-03	4.77933E-03	4.99E-03	1.91E-03	7.72679E+01	B+
NIST [18]	417.258	4.4E-03					E
$3s\ 3p\ ^3P_1^o - 3p^2\ ^1D_2$							
VV RCI	311.58	8.23087E-02	8.38464E-02	4.22E-02	3.80E-02	1.53516E+02	A+
VV+CV+C RCI int	312.30	9.14394E-02	9.21971E-02	4.68E-02	2.51E-02	3.43440E+02	AA
VV+CV+C RCI	312.30	9.14393E-02	9.21978E-02	4.68E-02	2.51E-02	3.43121E+02	AA
VV+CV+C+CC RCI int	311.95	8.99187E-02	9.02371E-02	4.58E-02	2.44E-02	8.00907E+02	AA
VV+CV+C+CC RCI	311.95	8.99279E-02	9.02746E-02	4.58E-02	2.44E-02	7.35835E+02	AA
RCI (RSMBPT) 100%	311.95	8.99269E-02	9.02691E-02	4.58E-02	2.44E-02	7.45469E+02	AA
RCI (RSMBPT) 100% int	311.95	8.99186E-02	9.02377E-02	4.58E-02	2.44E-02	7.99079E+02	AA
RCI (RSMBPT) 99.95%	311.96	8.99048E-02	9.02339E-02	4.58E-02	2.44E-02	7.74715E+02	AA
RCI (RSMBPT) 99.95% int	311.96	8.98970E-02	9.02085E-02	4.58E-02	2.44E-02	8.18511E+02	AA
RCI (RSMBPT) 99.5%	311.98	8.98396E-02	9.03289E-02	4.58E-02	2.44E-02	5.21358E+02	AA
RCI (RSMBPT) 99.5% int	311.98	8.98320E-02	9.02995E-02	4.58E-02	2.44E-02	5.45616E+02	AA
RCI (RSMBPT) 99%	311.97	8.97719E-02	9.04057E-02	4.57E-02	2.45E-02	4.02754E+02	AA
RCI (RSMBPT) 99% int	311.96	8.97646E-02	9.03791E-02	4.57E-02	2.45E-02	4.15255E+02	AA
RCI (RSMBPT) 95%	311.99	8.97523E-02	9.00675E-02	4.58E-02	2.48E-02	8.07672E+02	AA
RCI (RSMBPT) 95% int	311.99	8.97460E-02	9.00471E-02	4.58E-02	2.48E-02	8.45346E+02	AA
NIST [18]	312.556	8.3E-02					E

correlations are included, the line strength in the Babushkin gauge is close to the 8.9E-02 a.u. value. Therefore, using the RSMBPT method to include the CV, C, and CC correlations is more efficient than the regular method because it allows one to estimate the impact of the correlations and include the most important correlations types rather than the whole group of correlations. The use of the RSMBPT method for the inclusion of CV, C, and CC correlations also significantly reduces the CSF space and therefore for a more complex atom or ion allows inclusion of all types of correlations which is not always possible in regular GRASP2018 calculations. Thus, the QQE method provides a more accurate estimate of the errors in the case when the RSMBPT method is used.

The line strengths from the present computations are similar to those provided by NIST. Most of the line strengths agree better when only VV correlations are included (**VV RCI** strategy), and not when all types of the correlations are taken into account. Also it should be mentioned that the line strengths

given in the NIST are assigned with a worse accuracy class than in the present computations.

Figure 7 presents the comparison of all line strengths from the regular GRASP2018 calculations (**VV+CV+C+CC RCI int**) with the results from the **CV+C+CC RCI (RSMBPT) int** strategy when 100% of the CV, C and CC correlations are included. The line strengths are compared in the Babushkin gauge. It is seen that the line strengths obtained using the RSMBPT method reproduce the results of the regular calculations. The line strengths between the two calculations fully agree for most of the transitions, and differ only to within 0.18% for some of the weakest transitions.

Figure 8 presents the comparison of all line strengths from the regular GRASP2018 calculations (**VV+CV+C+CC RCI int**) with the results from the **CV+C+CC RCI (RSMBPT) int** strategy when 99.95 and 99% of the CV, C and CC correlations are included. The weakest transition ($S = 1.07E-08$) is excluded in the case of 99%, as the natural logarithm ratio for this transition is

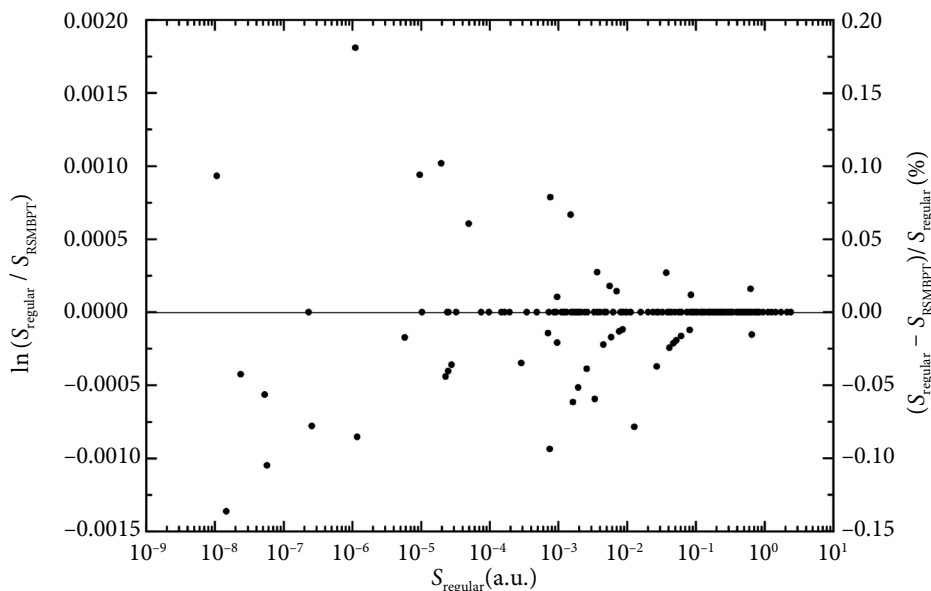


Fig. 7. Comparison of all line strengths from the regular GRASP2018 calculations (VV+CV+C+CC RCI **int**) with the results from the CV+C+CC RCI (R SMBPT) **int** strategy when 100% of the CV, C and CC correlations are included. The line strengths are compared in the Babushkin gauge.

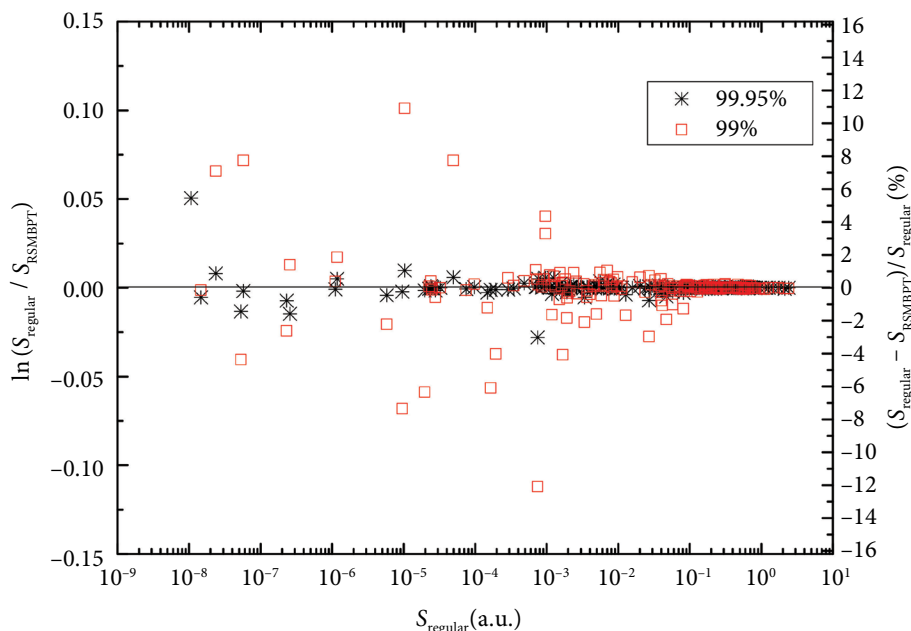


Fig. 8. Comparison of all line strengths from the regular GRASP2018 calculations (VV+CV+C+CC RCI **int**) with the results from the CV+C+CC RCI (R SMBPT) **int** strategy when 99.95 and 99% of the CV, C and CC correlations are included. The line strengths are compared in the Babushkin gauge.

equal to 0.36. The line strengths between the regular GRASP2018 calculations and the calculations using the R SMBPT method (cases 99.95 and 99%) agree well for most of the transitions. In the case of 99.95%, the discrepancy between two calcula-

tions is only up to 1.5%, except for two transitions where it reaches 2.8 and 5.2%. In the case of 99%, the strongest transitions agree very well between two calculations, the discrepancy for weaker transitions reaches up to 12% for some lines.

Figure 9 shows the statistical distribution of all computed E1 transitions by accuracy classes according to the computational schemes using the regular GRASP2018 method. It can be seen that the inclusion of the CV and C correlations improves the agreement between the Babushkin and Coulomb gauges. By adding the CC correlations, the number of tran-

sitions assigned with the AA accuracy class slightly reduces, and in the B+ accuracy class it increases.

Figure 10 shows the statistical distributions of all computed E1 transitions by accuracy class when CV, C and CC correlations with a different percentage of correlations is included using the RSMBPT method and using the regular GRASP2018 computational

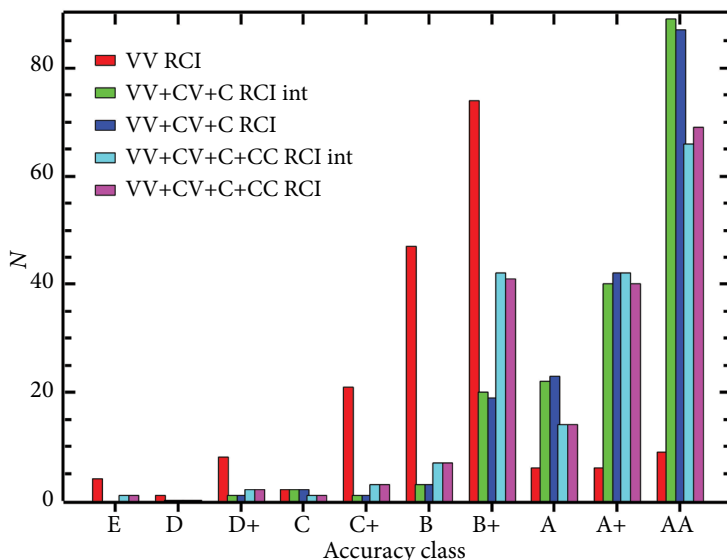


Fig. 9. Distribution of E1 transitions over the accuracy classes according to the computational schemes.

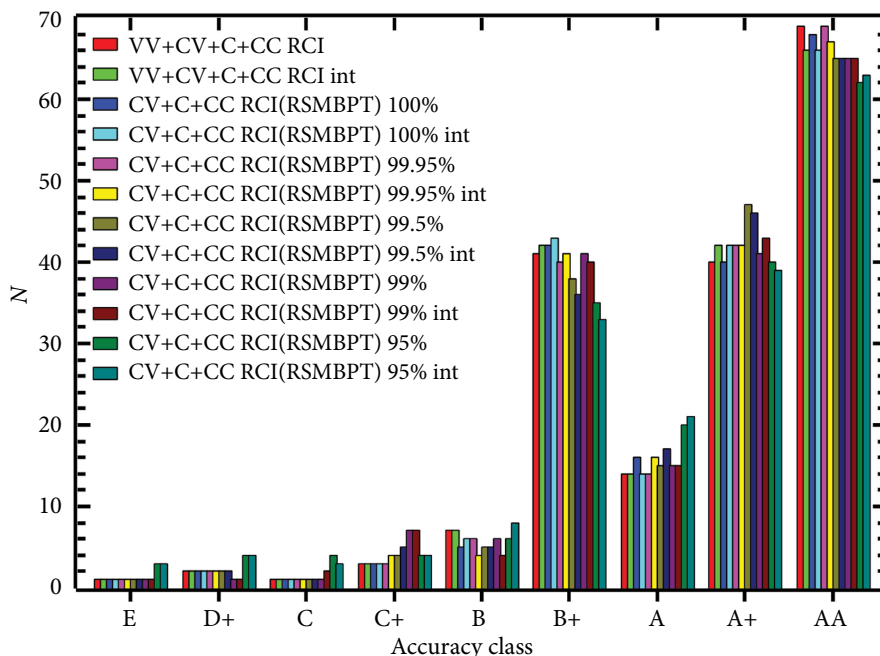


Fig. 10. Distribution of E1 transitions over the accuracy classes according to the computational schemes. The results from regular GRASP2018 calculations are compared with the results using RSMBPT when a different amount of CV, C and CC correlations are included.

scheme. It is seen that the transition distributions by accuracy classes are similar in both these methods, and remain similar when the configurations of CV, C and CC correlations with the smallest impact are neglected.

5. Conclusions

The method based on the Rayleigh–Schrödinger perturbation theory in an irreducible tensorial form is extended to take into account the CC correlations, providing the expressions for the estimation of these correlations. This extended RSMBPT method allows one to estimate the contribution of any K' configuration of the CV, C and CC correlations with a preferred core and virtual orbitals sets for any atom or ion.

The combination of RCI and the RSMBPT methods works perfectly for the calculations of energy and transition parameters when the CV, C and CC correlations are included using the RSMBPT method, as shown in the examples. The developed method has an advantage over the regular method because it allows the selection of the most relevant CV, C and CC correlations and significantly reduces the CSF space. Furthermore, the RSMBPT method allows the inclusion of correlations that cannot be included using the regular GRASP2018 calculation scheme. The abovementioned advantages of the RSMBPT method over the regular method would be useful and beneficial for calculations involving complex atoms and ions.

The change in CFs was observed when a new group of correlations was added to the regular GRASP2018 calculations. Meanwhile using the RSMBPT method, the values of CF are stable when the most important configurations of CV, C and CC correlations with a different amount of these correlations are included. This indicates that the most important correlations are included in the calculations and the line strengths would not change. Thus, the QQE method should provide a more accurate estimate of the uncertainties when the RSMBPT method is used. This is another advantage of the developed method over the regular GRASP2018 approach.

References

[1] G. Gaigalas, P. Rynkun, and L. Kitovienė, Second-order Rayleigh–Schrödinger perturbation theory for the GRASP2018 package: Core–valence corre-

lations, Lith. J. Phys. **64**(1), 20–39 (2024), <https://doi.org/10.3952/physics.2024.64.1.3>

- [2] G. Gaigalas, P. Rynkun, and L. Kitovienė, Second order of Rayleigh–Schrödinger perturbation theory for the GRASP2018 package: Core correlations, Lith. J. Phys. **64**(2), 73–81 (2024), <https://doi.org/10.3952/physics.2024.64.2.1>
- [3] I.P. Grant, *Relativistic Quantum Theory of Atoms and Molecules* (Springer, New York, 2007).
- [4] C. Froese Fischer, M. Godefroid, T. Brage, P. Jönsson, and G. Gaigalas, Advanced multiconfiguration methods for complex atoms: I. Energies and wave functions, J. Phys. B **49**(18), 182004 (2016), <https://doi.org/10.1088/0953-4075/49/18/182004>
- [5] I. Lindgren and J. Morrison, *Atomic Many-body Theory* (Springer-Verlag Berlin Heidelberg, New York, 1982).
- [6] G. Merkelis, G. Gaigalas, and Z. Rudzikas, Irreducible tensorial form of the effective Hamiltonian of an atom and the diagrammatic representation in the first two orders of the stationary perturbation theory, Liet. Fiz. Rink. (Sov. Phys. Coll.) **25**, 14–31 (1985) [in Russian].
- [7] G. Merkelis, G. Gaigalas, J. Kaniauskas, and Z. Rudzikas, Application of the graphical method of the angular momentum theory to the study of the stationary perturbation series, Izvest. Acad. Nauk SSSR, Phys. Coll. **50**, 1403–1410 (1986) [in Russian].
- [8] G. Gaigalas, *Irreducible Tensorial Form of the Stationary Perturbation Theory for Atoms and Ions with Open Shells*, PhD Thesis (Institute of Physics, Vilnius, 1989) [in Russian].
- [9] P. Jönsson, G. Gaigalas, J. Bieroń, C. Froese Fischer, and I.P. Grant, New version: GRASP2K relativistic atomic structure package, Comput. Phys. Commun. **184**(9), 2197–2203 (2013), <https://doi.org/10.1016/j.cpc.2013.02.016>
- [10] C. Froese Fischer, G. Gaigalas, P. Jönsson, and J. Bieroń, GRASP2018 – A Fortran 95 version of the general relativistic atomic structure package, Comput. Phys. Commun. **237**, 184–187 (2019), <https://doi.org/10.1016/j.cpc.2018.10.032>
- [11] P. Jönsson, M. Godefroid, G. Gaigalas, J. Ekman, J. Grumer, W. Li, J. Li, T. Brage, I.P. Grant, J. Bieroń,

- and C. Froese Fischer, An introduction to relativistic theory as implemented in GRASP, *Atoms* **11**, 7 (2023), <https://doi.org/10.3390/atoms11010007>
- [12] G. Gaigalas, A program library for computing pure spin-angular coefficients for one- and two-particle operators in relativistic atomic theory, *Atoms* **10**(4), 129 (2022), <https://doi.org/10.3390/atoms10040129>
- [13] G. Gaigalas and Z. Rudzikas, On the secondly quantized theory of the many-electron atom, *J. Phys. B* **29**(15), 3303 (1996), <https://doi.org/10.1088/0953-4075/29/15/007>
- [14] G. Gaigalas, Z. Rudzikas, and C. Froese Fischer, An efficient approach for spin-angular integrations in atomic structure calculations, *J. Phys. B* **30**(17), 3747 (1997), <https://doi.org/10.1088/0953-4075/30/17/006>
- [15] G. Gaigalas, O. Scharf, and S. Fritzsche, Maple procedures for the coupling of angular momenta. VIII. Spin-angular coefficients for single-shell configurations, *Comput. Phys. Commun.* **166**, 141–169 (2005), <https://doi.org/10.1016/j.cpc.2004.11.003>
- [16] Y.T. Li, K. Wang, R. Si, M. Godefroid, G. Gaigalas, Ch.Y. Chen, and P. Jönsson, Reducing the computational load – atomic multiconfiguration calculations based on configuration state function generators, *Comput. Phys. Commun.* **283**, 108562 (2023), <https://doi.org/10.1016/j.cpc.2022.108562>
- [17] P. Jönsson, G. Gaigalas, Ch. F. Fischer, J. Bieroń, I.P. Grant, T. Brage, J. Ekman, M. Godefroid, J. Grumer, J. Li, and W. Li, GRASP manual for users, *Atoms* **11**, 68 (2023), <https://doi.org/10.3390/atoms11040068>
- [18] A. Kramida, Yu. Ralchenko, J. Reader, and NIST ASD Team (2023), *NIST Atomic Spectra Database, Version 5.11* (National Institute of Standards and Technology, Gaithersburg, MD), <https://physics.nist.gov/asd>
- [19] P. Rynkun, S. Banerjee, G. Gaigalas, M. Tanaka, L. Radžiūtė, and D. Kato, Theoretical investigation of energy levels and transition for Ce IV, *Astron. Astrophys.* **658**, A82 (2022), <https://doi.org/10.1051/0004-6361/202141513>
- [20] G. Gaigalas, P. Rynkun, S. Banerjee, M. Tanaka, D. Kato, and L. Radžiūtė, Theoretical investigation of energy levels and transition for Pr IV, *MNRAS* **517**, 281 (2022), <https://doi.org/10.1093/mnras/stac2401>
- [21] R.D. Cowan, *The Theory of Atomic Structure and Spectra* (University of California Press, Berkeley, CA, USA, 1981).

ANTROSIOS EILĖS RELĖJAUS IR ŠRĖDINGERIO TRIKDYMŲ TEORIJA GRASP2018 PROGRAMINIAM PAKETUI: KAMIENO–KAMIENO KORELIACIJOS*

G. Gaigalas, P. Rynkun, L. Kitovienė

Vilniaus universiteto Teorinės fizikos ir astronomijos institutas, Vilnius, Lietuva

Santrauka

GRASP programinis paketas grindžiamas reliatyvistinės superpozicijos metodu, kuriuo tikslūs skaičiavimai atliekami, kai į juos įtraukiamos valentinės–valentinės, kamieno–valentinės, kamieno ir kamieno–kamieno elektronų koreliacijos per konfigūracinių būsenų funkcijas (KBF). Tai veda prie didelės KBF erdvės, todėl pagal šį metodą sunkiau atlikti pačius skaičiavimus. Darbe pristatomas tolesnis antrosios eilės trikdymų teorija grįsto metodo (G. Gaigalas, P. Rynkun, L. Kitovienė, Second-order Rayleigh–Schrödinger perturbation theory for the GRASP2018 package: Core–valence correlations, Lith. J. Phys. 64(1), 20–39 (2024), <https://doi.org/10.3952/physics.2024.64.1.3>) ir (G. Gaigalas, P. Rynkun, L. Kitovienė, Second-order Rayleigh–Schrödinger perturbation theory for the GRASP2018 package: Core correlations, Lith. J. Phys. 64(2), 73–81 (2024), <https://doi.org/10.3952/physics.2024.64.2.1>),

skirto svarbiausioms KBF, turinčioms didžiausią įtaką kamieno–valentinėms, kamieno ir kamieno–kamieno koreliacijoms, surasti, tobulinimas. Šis metodas paremtas reliatyvistinės superpozicijos ir stacionariosios antrosios eilės Relėjaus ir Šrėdingerio daugelio kūnų trikdymų teorijos neredukuotinėje tensorinėje formoje metodų deriniu.

Darbe pateiktame trikdymų teorijos išplėtime atsižvelgiama į elektronų kamieno–valentines, kamieno ir kamieno–kamieno koreliacijas, kai atomas ar jonas turi bet kokį valentinių elektronų skaičių. O į kitas koreliacijas jame atsižvelgiama tradiciniu būdu. Tai leidžia gerokai sumažinti KBF erdvę skaičiuojant sudėtingų atomų ir jonų įvairias charakteristikas. Taip pat darbe pateikiamas pavyzdys, parodantis, kaip šiuo metodu atlikti Fe XV jono energijos spektro struktūros ir E1 šuolių charakteristikų skaičiavimus.

* Skiriama šiuolaikinės teorinės fizikos Lietuvoje pradininko, „Lietuvos fizikos rinkinio“ iniciatoriaus akad. **Adolfo Jucio** (1904–1974) gimimo ir mirties sukaktims paminėti.